þÿ L u e n h a p i c r i t e s , C e n t r a l M o z a m b i q u e M e s s e n g mantle plume source of Karoo continental flood basalts?

Turunen, Sanni T.

2019-11-15

Turunen , S T , Luttinen , A V , Heinonen , J S & Jamal , D L 2019 , ' Luenha picrites, Central
þÿ M o z a m b i q u e M e s s e n g e r s f r o m a m a n t l e p l u m e s o u r c e o f K a r o o c o n t i n
' , Lithos , vol. 346-347 , 105152 . https://doi.org/10.1016/j.lithos.2019.105152

http://hdl.handle.net/10138/306192
https://doi.org/10.1016/j.lithos.2019.105152

Lithos 346–347 (2019) 105152

Contents lists available at ScienceDirect

Lithos

journal homepage: www.elsevier.com/locate/lithos

Luenha picrites, Central Mozambique – Messengers from a mantle plume source of Karoo continental flood basalts?

Sanni T. Turunen [a,*], Arto V. Luttinen [a], Jussi S. Heinonen [b], Daúd L. Jamal [c]

[a] Finnish Museum of Natural History, Geological Collections, P.O. Box 44, University of Helsinki, 00014, Finland
[b] Department of Geosciences and Geography, P.O. Box 64, University of Helsinki, 00014, Finland
[c] Department of Geology, Eduardo Mondlane University, Av. Moçambique km 1.5, Caixa Postal 257, Maputo, Mozambique

ARTICLE INFO

Article history:
Received 24 January 2019
Accepted 20 July 2019
Available online 25 July 2019

Keywords:
Picrite
Flood basalt
Mantle source
Large igneous province
Mantle plume

ABSTRACT

We present geochemical and isotopic (Nd, Sr) data for a picrite lava suite from the Luenha River and adjacent areas in Mozambique. The Luenha picrites represent a previously unknown type of picrites related to the Karoo large igneous province (LIP) and are distinguished by their notably low TiO_2 contents (0.3–1.0 wt%) and coupling of high Nb/Y with low Zr/Y and Sm/Yb. Relatively high CaO and low Zn/Fe point to a peridotitic mantle source. Contamination-sensitive incompatible element ratios show that one lava flow is likely to be uncontaminated by the crust and its composition suggests a mantle source with primitive mantle-like incompatible element ratios and mildly depleted isotopic ratios (initial $^{87}Sr/^{86}Sr = 0.7041$ and $\varepsilon_{Nd} = +1.4$ at 180 Ma). The primary melts of the Luenha picrites had MgO contents in the range of 13–21 wt%. Our preferred estimate for a primary melt composition (MgO = 18 wt%) resembles experimental melts of fertile mantle peridotite at 3–4 GPa and indicates liquidus temperature of 1445–1582 °C. Geochemical similarities suggest the Luenha picrites were generated from the same overall primitive mantle-like reservoir that produced the main volume of Karoo flood basalts in the Karoo, Kalahari, and Zambezi basins, whereas the previously identified enriched and depleted (upper) mantle sources of Karoo picrite suites (Mwenezi, Antarctica) were subordinate sources for flood basalts. We propose that the Luenha picrites record melting of a hot, chemically primitive mantle plume source that may have been rooted in the sub-African large low shear velocity province boundary and that such a source might have been the most significant magma source in the Karoo LIP.

1. Introduction

The origin of continental flood basalts (CFBs) and their relationships to mantle reservoirs and dynamics are unsettled topics in Earth sciences. For example, the roles of mantle plumes (e. g., French and Romanowicz, 2015), subduction processes (e. g., Wang et al., 2015), and ancient non-chondritic primitive mantle reservoirs (e.g., Jackson and Carlson, 2011) in their formation are not clear. Generalizing, the erupted CFB magmas have been variably modified by differentiation processes (magma mixing, fractional crystallization, crustal contamination, and degassing). Thermodynamically constrained models of magmatic differentiation demonstrate that even minor amounts of incompatible element-enriched partial melts from wallrocks can have a major influence on the incompatible trace element and isotopic ratios of flood basalts (Bohrson and Spera, 2001). Consequently, the assessment of CFB mantle sources is critically dependent on studies of rare, picritic rock types that represent high-Mg primitive magmas that have not been strongly affected by differentiation.

The Karoo large igneous province (LIP) is a Mid-Jurassic (~182–183 Ma; Jourdan et al., 2008; Svensen et al., 2012) CFB province that was emplaced in southern Gondwana prior to the breakup between Africa and Antarctica. The province has been frequently considered as a plume-generated LIP (Burke and Dewey, 1973; Storey, 1995; Torsvik et al., 2010; White, 1997), but geochemical studies have generally not favored plume sources for it because of the compositional similarity between Karoo CFBs and continental lithosphere (Duncan et al., 1990; Ellam, 2006; Ellam and Cox, 1989; Jourdan et al., 2007; Luttinen and Furnes, 2000; Wang et al., 2015). Given that this geochemical 'lithosphere signature' in the Karoo and many other CFB provinces is probably at least partially related to contamination of ascending magmas by lithospheric wallrocks (Arndt and Christensen, 1992; Heinonen et al., 2016; Neumann et al., 2011), flood basalt compositions are generally unsuitable for geochemical characterization of the mantle sources in continental LIPs.

Previous studies have demonstrated that several different mantle sources are required for the Karoo LIP. Two contrasting mantle sources of Karoo CFBs have been identified based on Karoo picrites. One of them shows affinity to ancient enriched lithospheric mantle and crustal materials (Ellam, 2006; Harris et al., 2015; Kamenetsky et al., 2017), and

* Corresponding author.
E-mail address: sanni.turunen@helsinki.fi (S.T. Turunen).

https://doi.org/10.1016/j.lithos.2019.105152

the other to depleted upper mantle (Heinonen et al., 2010; Heinonen and Kurz, 2015). Recent examination of geochemical data for the Karoo LIP on provincial scale revealed, however, that these two sources cannot explain the generation of all magma types and that, in fact, up to more than50 vol% of the CFBs call for a third geochemically distinctive mantle source and that this source is likely to geochemically resemble primitive mantle (PM) (Luttinen, 2018).

Here we report major element, trace element, mineral chemical, and Nd and Sr isotopic data for a recently discovered suite of picritic Karoo lavas from the Luenha River area, central Mozambique. The Luenha picrites are geochemically different from the other Karoo picrite suites and reveal a previously unknown mantle source for the Karoo LIP. This source shows geochemical resemblance to PM and was typified by notably high temperatures. Geochemical similarities between the Luenha picrites and voluminous flood basalt magma types indicate that the Luenha picrites may record a significant mantle plume source of the Karoo LIP.

2. Geological background

2.1. Karoo large igneous province

Extrusive and intrusive rocks belonging to the Karoo LIP are widespread in southern Africa and are also found in western Dronning Maud Land, Antarctica (Fig. 1). Geochronological studies point to relatively rapid emplacement of the main volume of the magmas during the early stages of Gondwana breakup ca. 182–183 Ma ago (Duncan et al., 1997; Svensen et al., 2012). The timing of magmatic activity in different parts of the province is uncertain, however, as many stratigraphical units remain undated and as the high-precision ages for extrusive and intrusive rock types spread over a time period of ca. 10 Ma (Jourdan et al., 2005; Luttinen et al., 2015). The remnants of Karoo CFBs and related dikes and sills comprise a total volume of ca. 2 million km^3 (Cox, 1988), whereas the total volume of Karoo-related magmatism is estimated to be 5–10 million km^3 (White, 1997). Poor exposure in the Antarctic part of the province and the role of submarine seismically defined dipping reflectors (Fig. 1) result in considerable uncertainty in the volume estimates. The volcanic units of the Karoo LIP typically overlie the Permian to Early Jurassic sedimentary rocks of the Karoo, Kalahari, and Zambezi basins (Catuneanu et al., 2005; Oesterlen and Millsteed, 1994; Smith, 1990). The sill complexes and dyke swarms variably intrude the sedimentary rocks, the Karoo volcanic succession, and the crystalline basement. The crystalline basement is composed of Archean cratons (Kaapvaal, Zimbabwe and Grunehogna) and surrounding Proterozoic metamorphic belts (Namaqua–Natal–Maud belt) (Jacobs et al., 2008) (Fig. 1).

The Karoo LIP is dominated by subalkaline, low-Mg tholeiitic rock types (Bristow, 1984). High-Mg rock types (collectively referred to as picrites in this study) are common in the Mwenezi-Tuli region, southern Africa, and are also found in the Vestfjella and Ahlmannryggen areas in Antarctica (Ellam and Cox, 1989; Heinonen and Luttinen, 2008; Riley et al., 2005) (Fig. 1). Compositionally diverse basalts and picrites vary from mildly incompatible element-enriched low-Ti (TiO_2 ca. 0.5–2 wt %) to strongly enriched high-Ti (TiO_2 2–5 wt%) types and exhibit wide ranges of initial ε_{Nd} (from −19 to +8) and $^{87}Sr/^{86}Sr$ (0.7030–0.7132) values (see data compilation of Luttinen, 2018). The great geochemical variability is likely to stem from variable conditions of mantle melting, fractional crystallization, crustal contamination (Heinonen et al., 2016; Jourdan et al., 2007), mantle source heterogeneity, and interaction of the heterogeneous primary magmas with the base of the lithosphere (Ellam and Cox, 1991; Heinonen et al., 2014; Jourdan et al., 2007).

Luttinen (2018) recently showed that the numerous Karoo magma types fall into two geochemically and geographically distinctive categories: A bilateral geochemical provincial pattern can be recognized by enrichment or depletion of Nb relative to Zr and Y. The extrusive and intrusive rock types of the Karoo, Kalahari, and Zambezi basins (Fig. 1) are characterized by higher Nb/Y at given Zr/Y than the extrusive and intrusive rock types elsewhere in the Karoo LIP. The variability in Nb/Y

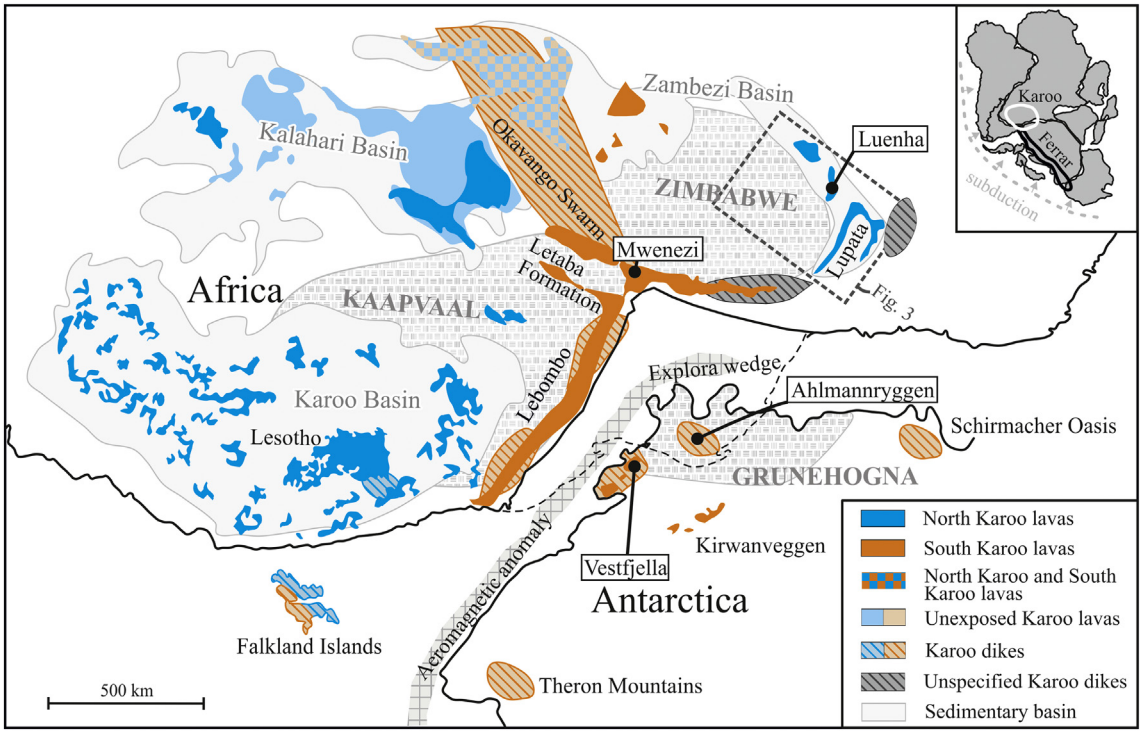

Fig. 1. Distribution of the Karoo LIP in reconstructed Gondwana supercontinent (inset) at 180 Ma. Occurrences of picrites are indicated with text boxes. The geochemically distinct North Karoo and South Karoo subprovinces are shown in blue and orange, respectively. Distribution of the Archaean Kaapvaal, Zimbabwe and Grunehogna cratons, Permian to Early Jurassic Kalahari, Karoo and Zambezi sedimentary basins, and geophysically detected Karoo-related anomalies are shown. Area of Fig. 3 is indicated by a dotted line rectangle. The map has been modified from Luttinen (2018). (For interpretation of the references to colour in this figure legend, the reader is referred to the web version of this article.)

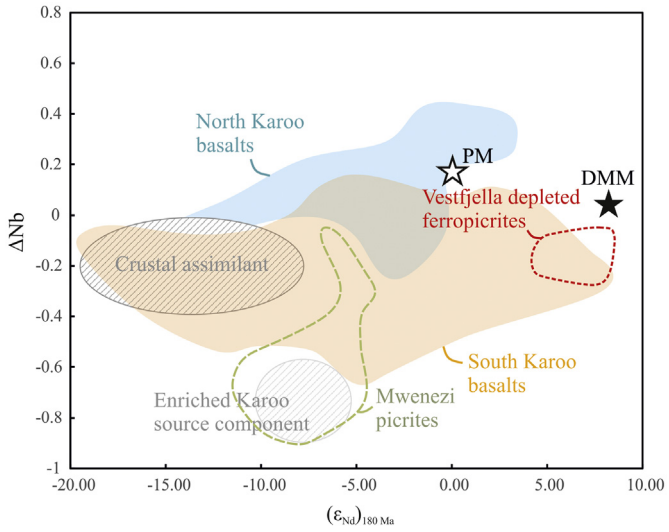

Fig. 2. ΔNb vs. initial εNd (180 Ma) variation diagram for the North Karoo and South Karoo flood basalts. Compositions of the Mwenezi picrites (Ellam and Cox, 1989) and the Vestfjella depleted ferropicrites (Heinonen et al., 2010; Heinonen and Luttinen, 2008) are shown for comparison. DMM is depleted MORB mantle (Workman and Hart, 2005) and PM is primitive mantle (Jacobsen and Wasserburg, 1980; Sun and McDonough, 1989). Compositions of plausible mantle sources of the enriched Mwenezi picrites (Enriched Karoo source component) and crustal assimilants are illustrated. Data for the Karoo flood basalts are from the compilation of Luttinen (2018). ΔNb = 1.74 + log (Nb/Y) – 1.92 log (Zr/Y) (Fitton et al., 1997).

(relative Nb-enrichment or -depletion) at given Zr/Y can be quantified using ΔNb values (Fitton et al., 1997; Fig. 2). Following the division of Luttinen (2018), the high-ΔNb (0.11 ± 0.11; average ± 1std; n = 271) CFBs within the great sedimentary basins constitute the North Karoo sub-province and the low-ΔNb (−0.21 ± 0.18; n = 548) CFBs of the the Karoo triple rift (African rifted margin, the Okavango dyke swarm, and Antarctica) make up the South Karoo sub-province (Figs. 1–2).

2.2. Karoo magmatism in Mozambique

The Karoo CFBs of Mozambique are widespread but little-studied. They are found in three main areas in southern and central Mozambique. Two occurrences are associated with the African rifted margin (Fig. 1). In southern Mozambique, the seaward-dipping CFB succession of the Lebombo Monocline is capped by the mafic and silicic rocks of the Movene Formation (Manninen et al., 2008; Melluso et al., 2008) and, in central Mozambique, the Sabi Monocline is made of seaward-dipping mafic lavas and coast-parallel mafic dykes (Manninen et al., 2008) (Fig. 1). The few published geochemical data for the mafic lavas and dykes of the Movene and Sabi successions indicate overall similarity to the Karoo CFBs of the Lebombo monocline (Manninen et al., 2008; Melluso et al., 2008) and support grouping of these mafic rock types as South Karoo CFBs (Luttinen, 2018) (Fig. 1). Reliable age data for the Sabi and Movene CFBs are lacking.

The Lupata trough and the Moatize-Luia graben (Fig. 3) in central Mozambique host mafic lavas and subordinate silicic volcanic rocks (Manninen et al., 2008). Both synforms are associated with the Zambezi basin (Fig. 1). Available geochemical data (Manninen et al., 2008) support grouping of the basalts into North Karoo (Luttinen, 2018; Fig. 1). The silicic volcanic rocks have yielded U-Pb zircon ages of ~180–188 Ma (Puttonen, 2016) which link the emplacement of the bimodal volcanic suites of the study area to the main eruptive phase of Karoo magmatism.

The crystalline basement in the Zambezi region consists predominantly of Proterozoic felsic and mafic intrusive rocks which are surrounded in the southwest by Archean granitoids and gneisses of the Zimbabwe Craton (Koistinen et al., 2008) (Fig. 3). Proterozoic to Mesozoic Pre-Karoo metasedimentary and sedimentary rock types occasionally cover the basement. Karoo lavas in the Lupata region directly overlie sandstones and carbonaceous mudstones of the Lower Karoo-age Matinde Formation (Fernandes et al., 2015), and are widely covered by younger sedimentary deposits (Manninen et al., 2008). Bicca et al. (2017) suggested that the Moatize graben is linked to a fault system that served as a magma pathway during Gondwana breakup.

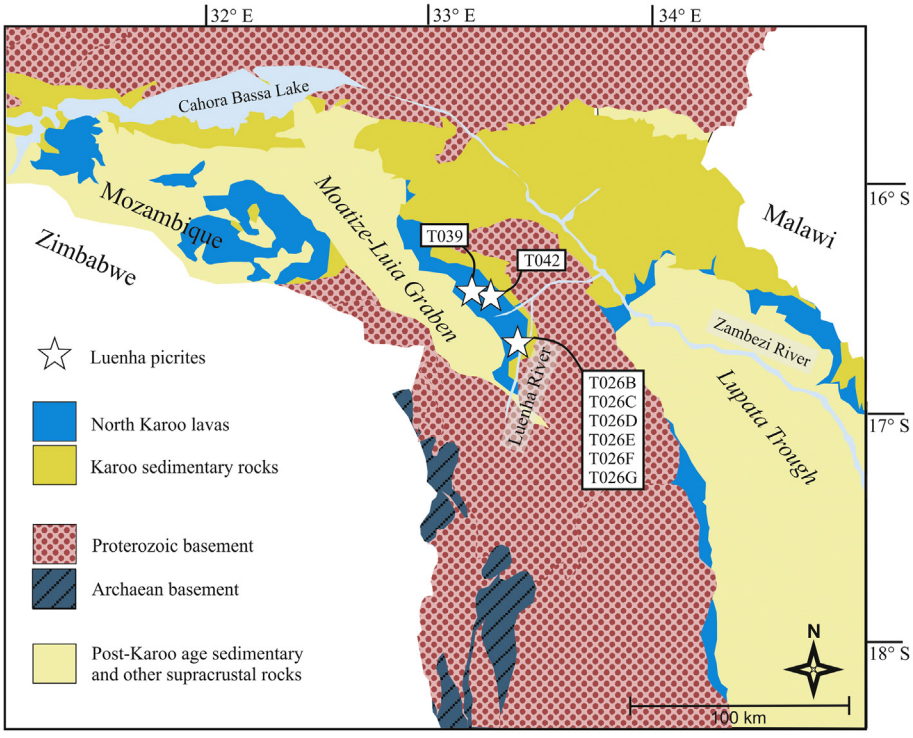

Fig. 3. A simplified bedrock map of northwestern Mozambique with the occurrences of the Luenha picrites and the North Karoo flood basalts (Luttinen, 2018) indicated. The map has been modified from Manninen et al. (2008).

2.3. Karoo picrites and their mantle sources

Recent studies on the mantle sources of Karoo magmatism have focused on picrites of the Karoo triple rift structure (Fig. 1). These are spatially and geochemically associated with the Nb-depleted South Karoo sub-province (Luttinen, 2018; Figs. 1–2).

In Africa, the Mwenezi and Tuli picrites of the Letaba Formation show a wide range of compositions from strongly incompatible-element-enriched (high-Ti) and potassic (molar K_2O/Na_2O mainly 1–1.7, but up to 8) to moderately enriched (low-Ti) and sodic (molar $K_2O/Na_2O < 1$) basalts and picrites (MgO = 8–26 wt%) (Ellam and Cox, 1989). The variable compositions and broad correlations between incompatible element concentrations and isotopic ratios have been interpreted to record hybridization (e.g., Ellam, 2006; Ellam et al., 1992; Ellam and Cox, 1989 ; Sweeney et al., 1991). The strongly enriched Mwenezi picrites define the so-called high-K-Na end-member (Ellam and Cox, 1989; Sweeney et al., 1991). They have incompatible element ratios (e.g. typically La/Nb = 2–5, K_2O/TiO_2 = 0.5–1.3) and radiogenic isotope ratios (e.g. initial ε_{Nd} ca. −8 to −11; $^{87}Sr/^{86}Sr$ 0.704–0.705) typical of old, enriched crustal or sub-continental lithospheric mantle (SCLM) material (Ellam, 2006; Ellam et al., 1992; Ellam and Cox, 1989, 1991; Jourdan et al., 2007; Kamenetsky et al., 2017). The strongly incompatible element-enriched Mwenezi picrites are effectively buffered against crustal contamination, and therefore their compositions are likely to represent an enriched mantle source component for the Karoo LIP (Ellam and Cox, 1991) (Fig. 2). Oxygen isotopic ratios (Harris et al., 2015) and Ni concentrations in olivine (Howarth and Harris, 2017; Sobolev et al., 2007) suggest presence of recycled crustal material in the source of the strongly enriched Mwenezi picrites. Most studies have favored some kind of SCLM source (Ellam, 2006; Howarth and Harris, 2017), possibly generated by ancient addition of oceanic crust into SCLM (Harris et al., 2015), but it is also possible that the enriched source component was recycled crustal material in the convective upper mantle (Kamenetsky et al., 2017).

The less enriched varieties of the Letaba picrites range to low-Ti compositions and define the so-called low-K-Na end-member (Ellam and Cox, 1989; Sweeney et al., 1991). The low-K-Na end-member may represent a different, mildly enriched lithospheric component (Ellam, 2006), or it may record hybridization between the high-K-Na end-member and a relatively depleted component from the convective mantle (Duncan, 1987; Ellam and Cox, 1991; Sweeney et al., 1991). Extrapolation of the geochemical trends of the Letaba picrites has suggested such a convective mantle component to be mid-ocean ridge basalt (MORB)-like magma (Ellam and Cox, 1991), although large scatter and sparsity of data hamper characterization of the depleted component. While the strongly enriched high-K-Na Mwenezi picrites lack basaltic correlatives, the less enriched compositions show compositional overlap with CFBs (Fig. 2). Overall, many studies have considered that the enriched source of the Letaba picrites was an important magma source of strongly enriched Karoo CFBs (Sweeney et al., 1994; Jourdan et al., 2007).

Several types of distinct Karoo-related picrites are found in Dronning Maud Land, Antarctica. At the Vestfjella nunataks, the CFB lava succession contains rare picritic units that can be correlated with the enclosing low-Mg lavas and are likely to be similarly contaminated with the lithosphere (Heinonen et al., 2010, 2016; Luttinen et al., 1998; Luttinen and Furnes, 2000). A crosscutting intrusive suite includes minor swarms of picritic dikes. One swarm is composed of Fe-rich dykes which show a wide range of MgO (8–26 wt%) and TiO_2 contents (1.3–2.2 wt%) and has been dated at ca. 186 Ma (Heinonen and Luttinen, 2008; Luttinen et al., 2015). This so-called depleted Vestfjella ferropicrite suite has incompatible element and isotopic (Nd, Sr, Pb, Os, He) ratios that are similar to those of modern MORB of the Southwest Indian Ridge and are indicative of a depleted mantle (DM) source (e.g., initial ε_{Nd} up to +8, $^{87}Sr/^{86}Sr$ down to 0.7035; Heinonen et al., 2010; Heinonen and Kurz, 2015). Oxygen isotopic data on olivine point to variable subduction-related metasomatism of this source (Heinonen et al., 2018). Geochemical modeling indicates that the variably enriched (low-Ti and high-Ti) CFBs of the Antarctic rifted margin could have been derived from the same overall DM source by variable partial melting, fractional crystallization, and crustal contamination (Heinonen et al., 2016; Luttinen et al., 2015). Generation of some strongly enriched CFB types require additional involvement of SCLM melts (Heinonen et al., 2016; Luttinen et al., 2015).

Studies in Antarctica have also revealed minor picritic dyke suites which exhibit broad geochemical similarity to ocean island basalts (OIB). Three compositional types of these OIB-like high-Ti picrites (enriched ferropicrites at Vestfjella and Group 3 and Group 4 picrites at Ahlmannryggen; Riley et al., 2005; Heinonen and Luttinen, 2008) are geochemically distinctive from other Karoo magma types and their compositions (e.g. Nd, Sr, Pb, Os isotopes) point to significant pyroxenitic source components (Heinonen et al., 2010, 2013, 2014; Heinonen and Luttinen, 2010). Overall, they have been regarded to represent subordinate enriched mantle source components which have not been volumetrically significant sources of Karoo CFBs as a whole (Heinonen et al., 2010, 2014), and are thus not discussed further in this study.

In the case of the previously known Karoo LIP picrite occurrences, we focus our discussion and comparisons on the strongly enriched Mwenezi picrites and the Vestfjella depleted ferropicrites which reveal two distinct and important mantle sources for the Karoo LIP. The former shows affinity to ancient lithospheric material and the latter has been derived from DM sources (Ellam and Cox, 1989; Harris et al., 2015; Heinonen et al., 2016; Kamenetsky et al., 2017; Luttinen et al., 2015). The great compositional variability of the low-ΔNb South Karoo CFBs can be largely explained by variable hybridization and differentiation of magmas derived from these two predominant mantle reservoirs (Fig. 2; Ellam and Cox, 1991; Ellam et al., 1992; Luttinen et al., 2015; Heinonen et al., 2016). In contrast, Luttinen (2018) showed that the voluminous high-ΔNb North Karoo CFBs require a different kind of a mantle source typified by high ΔNb and mildly depleted isotopic composition (Fig. 2).

3. Samples and methods

3.1. Samples

This study focuses on samples of olivine-porphyritic lavas discovered by our team along the Luenha River and adjacent areas in the Moatize-Luia graben in 2012 (Fig. 3). The olivine-rich rocks from these locations are designated here as the Luenha picrites. A stratigraphically overlying rhyolite has been dated at 180 Ma using the U-Pb zircon method, which provides a minimum age for the picrites (Puttonen, 2016). Coordinates of the sampling sites are given in Table 1.

At the Luenha River, picritic lavas form a capping suite of a mildly (ca. 10°) southwest-tilting CFB lava succession. The schematic map of the outcrop and detailed images of the rocks are available in the Supplementary Figs. S1 and S2. Field observations suggest that the picrites represent ca. 60 m thick lava suite sandwiched between a thin (ca. 0.5 m) Jurassic paleosol at the base and a discordant sedimentary breccia unit at the top. The exposed lava succession along the Luenha River is composed of pahoehoe flow units with vesicular upper and lower parts and relatively vesicle-free cores. The orientation of the pipe vesicles indicates flow direction to northeast. The uppermost ca. 10 m thick part of the suite is made of thin (0.2 to <1 m) strongly altered flow lobes (unit I, not sampled). These are underlain in stratigraphic order by thicker units II (2.5 m), III (1 m), and IV (2 m). Units II and IV contain up to 60 cm long pipe vesicles at the base. Samples T026C, T026B, and T026D represent the vesicle-poor cores of the units II, III and IV, respectively. The underlying part of the suite is partially unexposed, and the stratigraphy between units IV and V is unexposed. The field observations give an impression of a monotonous ca. 40 m thick succession of picrite lavas consisting of units V (>1 m) and VI (>2 m). Sample T026E represents

Table 1
Major element oxide and trace element compositions, and coordinates of the Luenha picrites.

Sample	AL-T026B	AL-T026C	AL-T026D	AL-T026E	AL-T026F	AL-T026G	AL-T039	AL-T042
Latitude	S 16.69527	–	S 16.69541	S 16.69560	S 16.69613	–	S 16.44982	S 16.46258
Longitude	E 33.3447	–	E 33.3449	E 33.3454	E 33.3468	–	E 33.1889	E 33.2629
Elevation (m)	208	–	208	206	203	–	285	294
SiO_2	46.54	46.41	47.77	47.30	44.10	43.87	46.08	43.14
TiO_2	0.50	0.50	0.57	0.94	0.31	0.29	0.50	0.38
Al_2O_3	16.34	15.59	16.83	14.26	10.65	9.92	12.75	7.97
FeO_{tot}	8.27	8.85	9.38	11.56	9.55	10.21	9.84	10.62
MnO	0.15	0.16	0.12	0.18	0.16	0.17	0.17	0.17
MgO	8.94	10.50	7.22	9.18	23.57	25.00	17.22	26.83
CaO	12.21	11.78	13.33	11.51	8.03	7.80	9.96	6.74
Na_2O	1.49	1.45	1.79	1.98	1.01	0.93	1.17	0.78
K_2O	0.54	0.12	0.16	0.28	0.07	0.06	0.10	0.06
P_2O_5	0.04	0.05	0.05	0.11	0.03	0.03	0.05	0.03
LOI	4.98	4.44	2.38	2.12	1.56	0.94	2.02	2.23
Sum	100.01	99.85	99.60	99.43	99.03	99.21	99.84	98.95
Mg#	68.1	70.2	60.4	61.1	83.0	82.9	77.6	83.3
Cr	565	560	629	630	2309	2469	1583	2028
Ni	194	212	186	255	990	1057	646	1344
Sc	42.7	40.6	43.7	44.1	28.6	27.7	36.3	26.9
V	219	221	239	307	155	151	230	180
Cu	106	109	108	134	77	73	101	85
Zn	53	57	55	79	58	58	61	62
Ga	13.3	11.9	14.7	16.0	9.4	6.5	12.1	8.8
Ta	0.17	0.16	0.21	0.49	0.09	0.09	0.13	0.10
Nb	2.88	2.96	3.67	8.78	1.56	1.42	2.18	1.57
Hf	0.87	0.89	1.02	1.90	0.46	0.46	0.87	0.51
Zr	27.6	27.8	33.1	66.1	14.8	14.3	28.3	15.8
Y	15.60	15.41	17.71	25.81	9.58	9.23	15.65	10.74
Ba	1305	49	81	120	42	34	36	26
Rb	17.9	2.7	3.2	5.3	1.3	1.6	2.5	3.2
Sr	257	107	132	126	75	73	54	33
Cs	0.05	0.04	0.03	0.08	0.10	0.07	0.40	2.68
U	0.10	0.11	0.17	0.28	0.04	0.05	0.08	0.03
Th	0.63	0.64	0.80	1.72	0.25	0.24	0.54	0.14
Pb	0.63	0.68	0.92	1.43	0.29	0.31	0.51	0.15
La	3.60	3.70	4.45	9.48	1.80	1.75	2.80	1.09
Ce	7.31	7.50	8.97	18.93	3.71	3.59	5.84	2.42
Pr	0.97	0.98	1.16	2.35	0.48	0.47	0.78	0.34
Nd	4.40	4.37	5.17	9.95	2.30	2.20	3.68	1.91
Sm	1.41	1.45	1.67	2.86	0.81	0.80	1.40	0.91
Eu	0.58	0.60	0.68	1.06	0.36	0.35	0.54	0.41
Gd	2.05	2.12	2.42	3.81	1.22	1.20	2.11	1.57
Tb	0.42	0.42	0.48	0.71	0.26	0.24	0.41	0.31
Dy	2.80	2.87	3.19	4.76	1.76	1.65	2.82	2.05
Ho	0.62	0.63	0.70	1.02	0.39	0.37	0.62	0.43
Er	1.70	1.73	1.97	2.87	1.08	1.01	1.74	1.20
Tm	0.25	0.25	0.28	0.41	0.16	0.15	0.25	0.17
Yb	1.56	1.54	1.75	2.57	0.97	0.95	1.57	1.01
Lu	0.24	0.23	0.29	0.40	0.16	0.14	0.25	0.15

Major element oxides and trace elements Cr, Ni, V, Cu, Zn, and Ga have been measured with XRF and the other trace elements with ICP-MS. Major element oxides and LOI (loss on ignition) are reported in wt% and trace elements in ppm. $Mg\# = 100*Mg/(Mg + 0.9*FeO_{tot})$.

the vesicular upper crust of unit V, whereas samples T026F and T026G represent the vesicle poor flow core of unit VI. Sample T026G was collected from a field of large boulders adjacent to the underlying paleosol, the contact to which is unexposed .

Samples T039 and T042 were collected from two fields of picrite boulders that we interpret to represent in-situ weathering of lava flows. Judging from the size of the boulders and the lack of vesicles, the samples represent cores of at least 1 m thick flow units. The presently available field context does not provide enough detail to discriminate whether these units record individual picrite interlayers within a basaltic lava succession or represent more numerous picrite units.

3.2. Methods

The geochemical compositions of the lavas were analyzed from whole-rock samples removed with a hammer. Approximately 0.5 kg of each sample was crushed with a jaw crusher at the Department of Geosciences and Geography, University of Helsinki. Rock chips were washed in ion-exchanged water and dried at 105 °C. Representative rock chips were hand-picked for analysis avoiding steel streaks and chips, weathered surfaces, filled cavities and amygdules.

Analysis of major and trace element contents were performed at the Peter Hooper Geoanalytical Laboratory, Washington State University, using X-ray fluorescence (XRF) and inductively coupled plasma mass spectrometery (ICP-MS) methods. The part used for XRF analysis was pulverized with a tungsten carbide ball mill and the part for ICP-MS with an Fe-mill. The methods for XRF analysis are described by Johnson et al. (1999) and for ICP-MS by Knaack et al. (1994). The estimated precision for the XRF data is mainly <5% (relative standard deviation, RSD) and is comparable to compositional difference between two random samples from the same rock unit. The long-term precision for the ICP-MS data is typically <5% (RSD) for rare earth elements (REE) and < 10% for the remaining trace elements.

Results on duplicate analyses and chemical reference materials are listed in Supplementary Table S1. In the case of XRF data, the duplicate

analyses indicate precision of <2.5% for most major elements and < 5% for P_2O_5, < 5% for Ni, Cr and V, and < 15% for Ga, Cu and Zn. Analyses of BCR-1 and BHVO-1 references show that major elements and Ni, V, Ga and Zn are within 5% and Cr and Cu are within <35% and 20% of the recommended values. In the case of ICP-MS data, the duplicate analyses of the samples with low concentrations of incompatible elements indicate precision of <5% for most incompatible elements (including REE), and <20% for Ta and Pb. Analytical results of trace elements on BHVO-2 and BIR-1 are within 5% of the recommended values apart from Eu, Tb, Dy, Ho, Lu (< 10%), Ba, Nb, Pb (< 25%), and Th, U, Rb (< 40%) and Cs which shows a 254% deviation from the recommended values of the incompatible element poor BIR-1 standard. The error in ΔNb values, which have been calculated using ICP-MS data on Nb, Zr, and Y, is estimated to be below ±0.1 units.

For whole-rock Sr and Nd isotopic analysis, the hand-picked rock chips were ground using a tungsten carbide mill at the Department of Geosciences and Geography, University of Helsinki. The isotopic compositions were measured at the Finnish Geosciences Research Laboratory, Geological Survey of Finland. A 0.18 g batch of rock powder was placed in each polytetrafluoroethylene (PTFE) container with 2 ml of HF and a few drops of HNO_3. The solutions were left to dissolve in closed containers on a hot plate. After perfect dissolution, the sample was dried, and the residue was re-eluated with concentrated HNO_3, 6.2 N HCl and 2.5 N HCl. The solutions were then placed in test tubes, centrifuged, and the pellets were discarded. The liquid fractions were passed through resin ion exchange columns with controlled doses of 2.5 N HCl (0.5 ml, 1 ml, 1 ml, 15 ml, 12 ml and 6 ml). The Sr-enriched fraction was then collected using 15 ml of 2.5 N HCl. The columns were subsequenly rinsed with 10 ml of 2.5 N HCl, 2 ml of ultra-clean ion exchanged water, and 10 ml of 4 N HNO_3. The REE were then collected using 17 ml of 4 N HNO_3. Both Sr- and REE-enriched solutions were dried under infrared lamps in ventilated PTFE domes. The REE fractions were eluated with 0.5 ml of 0.23 N HCl and pipeted into ion exchange resin columns, and rinsed with the same solution in doses of 0.5 ml, 1 ml, 1 ml, 5 ml and 8 ml. The Nd-enriched solutions were collected using the last dose and were dried under infrared lamps.

Isotopic ratios were measured with a VG Sector 54 multicollector thermal ionization mass spectrometer (TIMS). Prior to the measurements, the Sr fractions were dissolved in one drop of 0.75 N H_3PO_4 and loaded on a Ta filament. The Nd fractions were dissolved in one drop of 0.15 N H_3PO_4 and loaded on the side filament of a Ta-Re-Ta triple filament unit. The acid was evaporated from the filaments using a 1.5 A electric current. During thermal ionization, a 2.5–3.0 A current was used for Sr and 2.7–3.2 A for Nd. The isotopic ratios were measured with several interchanging collectors during each measurement cycle. The Nd ratios were normalized to natural $^{146}Nd/^{144}Nd$ ratio of 0.7219 (O'Nions et al., 1977). Repeated analysis of the SRM981 and La Jolla standards yielded $^{87}Sr/^{86}Sr$ 0.710246 ± 0.000008 and $^{143}Nd/^{144}Nd$ 0.511850 ± 0.000011, respectively.

Isotopic analysis of $^{143}Nd/^{144}Nd$ in sample T042 failed to yield precise data (0.512784 ± 0.000201). The same TIMS instrument was not available for reanalysis due to shutdown of the facility. Therefore, the isotopic ratio of $^{143}Nd/^{144}Nd$ in sample T042 was measured with TIMS at the Department of Terrestial Magnetism, Carnegie Insitution for Science. Repeated measurement of the JNDi standard gave an average value of 0.512100 ± 0.000003, which corresponds to 0.511843 for La Jolla standard (Tanaka et al., 2000). The result for sample T042 ($^{143}Nd/^{144}Nd$ = 0.512825 ± 0.000009; Table 2) is within the uncertainty of the previously failed TIMS measurements. For detailed analytical procedure at the Department of Terrestrial Magnetism, the reader is referred to Heinonen et al. (2010).

Mineral compositions were determined with JEOL JXA-8600 electron probe microanalyzer equipped with SAMx hardware and XMAs/IDFix/Diss5 software at the Department of Geosciences and Geography, University of Helsinki. Wavelength dispersive spectroscopy (WDS) was used for quantitative analysis. Precision and accuracy data for the method have been reported by Heinonen et al. (2013). The thin sections were inspected optically and mapped for optimal analysis spots to avoid inclusions or fractures before carbon coating. In each analysis spot, three spots were analyzed in close proximity to each other with a 15 nA current and a 15 kV accelerating voltage. A representative average composition was then calculated for each spot to monitor mineral homogeneity. The oxide contents were calculated based on the stoichiometric formula of each analyzed mineral species. Results with anomalously low totals (less than ca. 97%) were discarded when calculating the averages.

4. Petrography and mineral chemistry

All of the Luenha picrite samples are porphyritic, with the phenocryst assemblages consisting in the interpreted order of crystallization of (1) olivine (sample T039), (2) olivine and spinel (samples T026G and T042) and (3) olivine, spinel and plagioclase (samples T026B–T026F). Olivine is the predominant phenocryst phase in the studied samples (10–50 vol%), whereas plagioclase and spinel phenocrysts are minor constituents (< 5 vol%). Water-bearing primary magmatic phases have not been observed. Mineral chemical data are listed in Supplementary Table S2 and petrographic photographs are shown in the Supplementary Fig. S2.

The euhedral to subhedral olivine phenocrysts are 1 to 10 mm long along c-axis. Sample T039 contains distinctively tabular olivine phenocrysts. Aggregates of olivine phenocrysts are found in many samples.

Table 2
Sr and Nd isotope compositions of the Luenha picrites.

Sample	AL-T026B	AL-T026C	AL-T026D	AL-T026E	AL-T026F	AL-T026G	AL-T039	AL-T042
Rb (ppm)	17.9	2.7	3.2	5.3	1.3	1.6	2.5	3.2
Sr (ppm)	257	107	132	126	75	73	54	33
Sm (ppm)	1.4	1.5	1.7	2.9	0.8	0.8	1.4	0.9
Nd (ppm)	4.4	4.4	5.2	10.0	2.3	2.2	3.7	1.9
$^{87}Rb/^{86}Sr$	0.19397	0.06889	0.06787	0.11618	0.04845	0.05946	0.13166	0.27459
$^{87}Sr/^{86}Sr$	0.710685	0.707000	0.708639	0.707202	0.707248	0.707617	0.704960	0.704799
2σ error	±0.000007	±0.000007	±0.000007	±0.000007	±0.000013	±0.000011	±0.000009	±0.000007
$(^{87}Sr/^{86}Sr)_{180Ma}$	0.710189	0.706823	0.708465	0.706904	0.707124	0.707465	0.704623	0.704096
	±0.000070	±0.000026	±0.000025	±0.000042	±0.000022	±0.000024	±0.000048	±0.000098
$^{147}Sm/^{144}Nd$	0.19341	0.20132	0.19585	0.17357	0.21371	0.21909	0.23004	0.28816
$^{143}Nd/^{144}Nd$	0.512625	0.512546	0.512610	0.512595	0.512688	0.512734	0.512680	0.512825
2σ error	±0.000005	±0.000021	±0.000005	±0.000013	±0.000005	±0.000033	±0.000006	±0.000009
$(^{143}Nd/^{144}Nd)_{180\ Ma}$	0.512397	0.512309	0.512379	0.512391	0.512436	0.512476	0.512409	0.512486
	±0.000044	±0.000050	±0.000045	±0.000042	±0.000049	±0.000060	±0.000053	±0.000066
$(\varepsilon_{Nd})_{180\ Ma}$	−0.3	−2.0	−0.7	−0.4	0.4	1.2	−0.1	1.4

TIMS data on $^{87}Sr/^{86}Sr$ and $^{143}Nd/^{144}Nd$ are normalized to $^{86}Sr/^{84}Sr = 0.1194$ and $^{146}Nd/^{144}Nd = 0.7219$, respectively. $^{87}Rb/^{86}Sr$ and $^{147}Sm/^{144}Nd$ are calculated on the basis of ICP-MS data on Rb, Sr, Sm, and Nd and e_{Nd} (180 Ma) is calculated using $^{143}Nd/^{144}Nd = 0.512638$ for the chondritic uniform reservoir. Errors in the initial $^{87}Sr/^{86}Sr$ and $^{143}Nd/^{144}Nd$ are based on analytical precision in TIMS and ICP-MS measurements.

Olivine is universally altered in the topmost units at Luenha River (samples T026B, T026C and T026D), but well preserved in the other samples. The analysis of fresh olivine shows high-Mg compositions in the cores ($Fo_{86–89}$), with the exception of sample T039 ($Fo_{77–79}$), and mild Fe-enrichment in the rims ($Fo_{80–87}$). The CaO concentration is usually 0.25–0.35 wt%, which is considered to be characteristic of volcanic olivine phenocrysts (e.g. Simkin and Smith, 1970). The translucent brown 0.5–5 mm sized spinel microphenocrysts (Cr# = 0.31–0.48; TiO_2 = 0.16–0.44 wt%; Al_2O_3 = 22.0–37.5 wt% in the cores) are found as euhedral inclusions in olivine and as independent phenocrysts. In the groundmass, the translucent spinel is mantled with opaque chromite, and chromite is also found as separate crystals. Olivine-hosted crystallized melt inclusions show similar anhydrous primary mineral assemblages as the host rock. Samples T026B, T026C, and T026E contain ca. 5 vol% of plagioclase phenocrysts (length 1–4 mm along c-axis). The plagioclase phenocrysts typically exhibit Ca-rich cores ($An_{72–87}$),

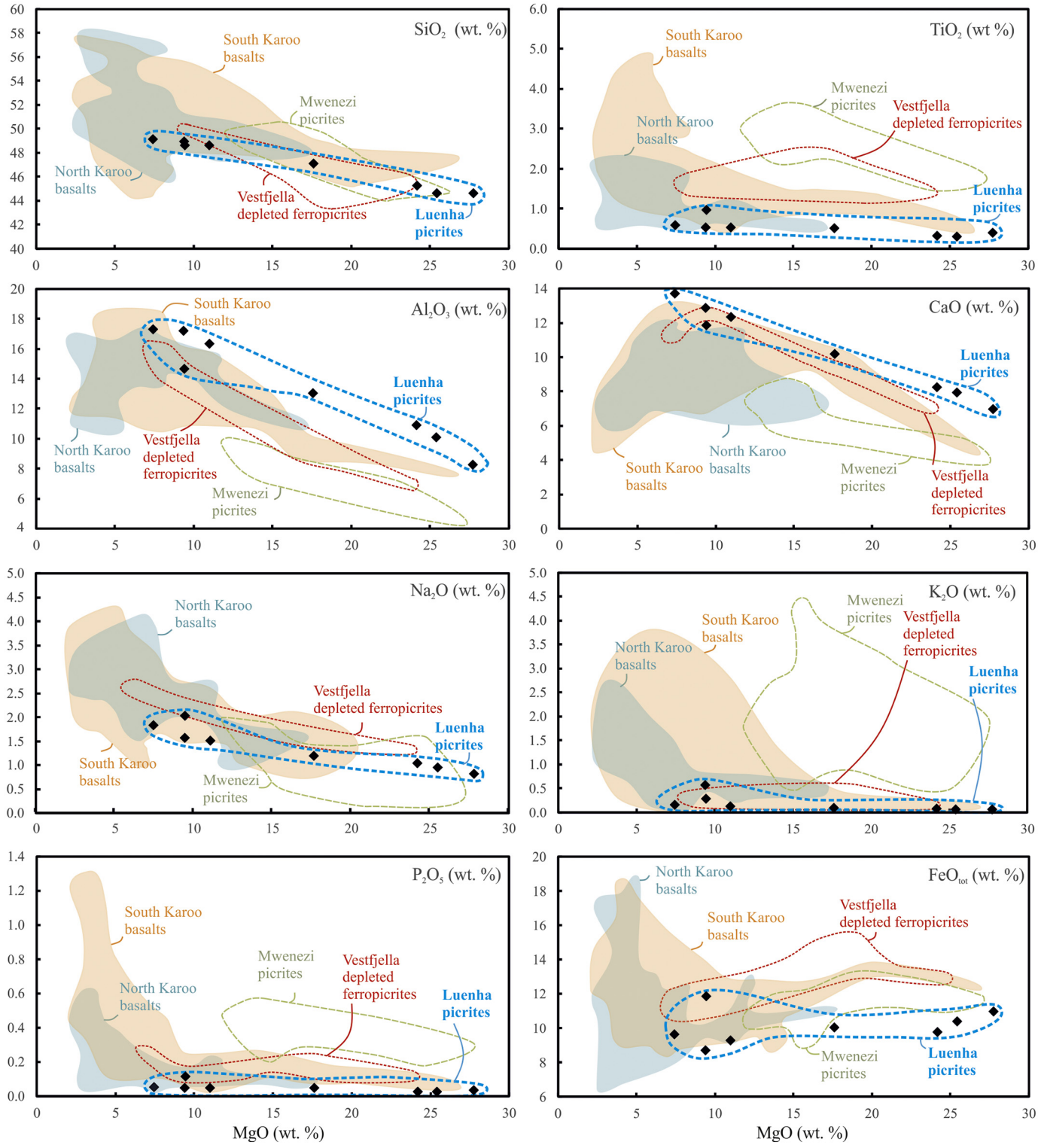

Fig. 4. Major element oxide variation diagrams for the Luenha picrites. Compositions of the North Karoo and South Karoo flood basalts (data compilation from Luttinen, 2018), Mwenezi picrites (Ellam and Cox, 1989), and Vestfjella depleted ferropicrites (Heinonen and Luttinen, 2008) are shown for comparison.

oscillatory zoning, and general decrease in Ca contents from core to rim. The plagioclase phenocrysts are generally quite fresh, but contain minor secondary sericite along fractures.

The groundmass consists of plagioclase ($An_{37–60}$), diopsidic to augitic clinopyroxene, Fe-Ti-Cr oxides, and mesostasis. The groundmass textures vary from ophitic (samples T026F, T026G, T042) to subophitic (samples T026B, T026C, T026D, T039) and intergranular (sample T026E). The single intergranular sample shows preferred orientation of plagioclase laths. Samples T026B–T026E contain intersertal parts with the mesostasis representing devitrified volcanic glass and < 1 vol % of small amygdules.

5. Geochemistry

5.1. Major and trace elements

The major and trace element compositions of the Luenha picrites are listed in Table 1. The Luenha picrites are subalkaline olivine-normative tholeiites. Compared to most Karoo CFBs, they are typified by higher MgO and lower TiO_2 and K_2O (Fig. 4). Three of the most magnesian samples (AL-T026F, AL-T026G, and AL-T042) are olivine cumulates (see Section 6.4.). One sample (AL-T039) is classified as a picrite and four samples (AL-T026B, AL-T026C, AL-T026D, and AL-T026E) as basalts according to the classification scheme for high-Mg volcanic rocks by Le Bas (2000) as recommended by the International Union of Geological Sciences (Table 1). Mg-number ($100*Mg/[Mg + 0.9*Fe_{tot}]$) varies from 60 to 83. The Luenha suite exhibits negative correlations of MgO against Al_2O_3, SiO_2, CaO, TiO_2 and Na_2O (Fig. 4).

Compatible trace elements Ni and Cr correlate positively with MgO and show high contents in general (Fig. 5). Incompatible trace element contents (e.g., Nb and Zr) are low and correlate negatively with MgO (Fig. 5). The PM-normalized REE patterns are generally flat, but, in detail, most patterns have a sinuous shape with low Pr and Nd, but also low Yb and Lu (Fig. 6a). Such a sinuous pattern is most pronounced in sample T042, which further shows slight depletion in all light REE relative to other REE.

The PM-normalized incompatible trace element patterns of the Luenha picrites are also relatively flat apart from negative Ti, P, and Zr anomalies (Fig. 6b). Overall, the PM-normalized REE and incompatible element patterns of the Luenha picrites show broad resemblance to enriched MORB (Fig. 6 a and b). Sample T042 is distinguished by its small positive Nb anomaly with $(Nb/La)_N$ of 1.4 (Fig. 6b).

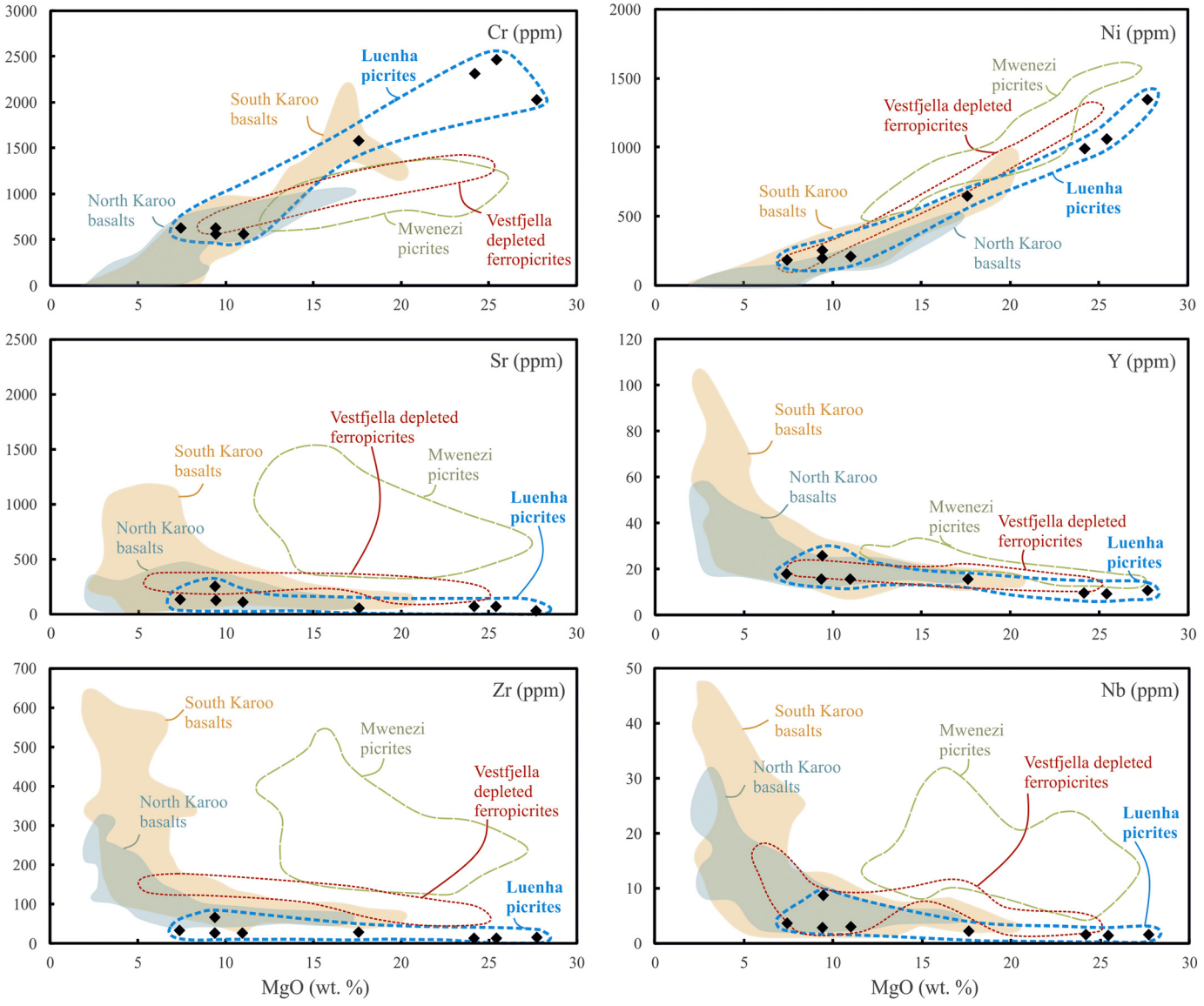

Fig. 5. Trace element variation diagrams for the Luenha picrites. Composition of the North Karoo and South Karoo flood basalts (data compilation from Luttinen, 2018), Mwenezi picrites (Ellam and Cox, 1989), and Vestfjella depleted ferropicrites (Heinonen and Luttinen, 2008) are shown for comparison.

Compared to the Mwenezi picrites and Vestfjella depleted ferropicrites, the Luenha picrites have significantly lower TiO_2 and higher Al_2O_3 at a given MgO (Fig. 4). The K_2O concentrations in Luenha picrites are low and roughly similar as in the Vestfjella depleted ferropicrites, but several times lower than those of the enriched Mwenezi picrites (Fig. 4). The incompatible trace element concentrations (e.g. Sr, Zr, and Nb) of the Luenha picrites are mainly lower than those in the Vestfjella depleted ferropicrites and the Mwenezi picrites (Fig. 5). The Cr concentrations of the Luenha picrites are typically higher, whereas the Ni concentrations are lower than in the Vestfjella depleted ferropicrites and the Mwenezi picrites at a given MgO content (Fig. 5).

5.2. Sr and Nd isotopes

Initial $^{87}Sr/^{86}Sr$ and $^{143}Nd/^{144}Nd$ isotopic ratios for the Luenha picrites were calculated at 180 Ma using $^{87}Rb/^{86}Sr$ and $^{147}Sm/^{144}Nd$ derived from the ICP-MS data (Table 2). The Luenha picrites exhibit a relatively narrow range of initial $^{143}Nd/^{144}Nd$ with initial ε_{Nd} values varying from −2.0 to +1.4 (Table 2), which are significantly higher than those of the Mwenezi picrites (−9.7 to −3.3; Ellam and Cox, 1989), but lower than those of the Vestfjella depleted ferropicrites (from +4.8 to +8.3; Heinonen et al., 2010). In comparison, the initial $^{87}Sr/^{86}Sr$ values of the Luenha picrites are much more variable, range from chondritic to strongly radiogenic (0.7041–0.7102), and overlap with the range of the Mwenezi picrites and the Vestfjella depleted ferropicrites (Fig. 7). The Luenha picrites comprise an array which is typified by variable initial $^{87}Sr/^{86}Sr$ at nearly constant chondritic initial ε_{Nd} and mainly plots outside the field of Karoo CFBs (Fig. 7).

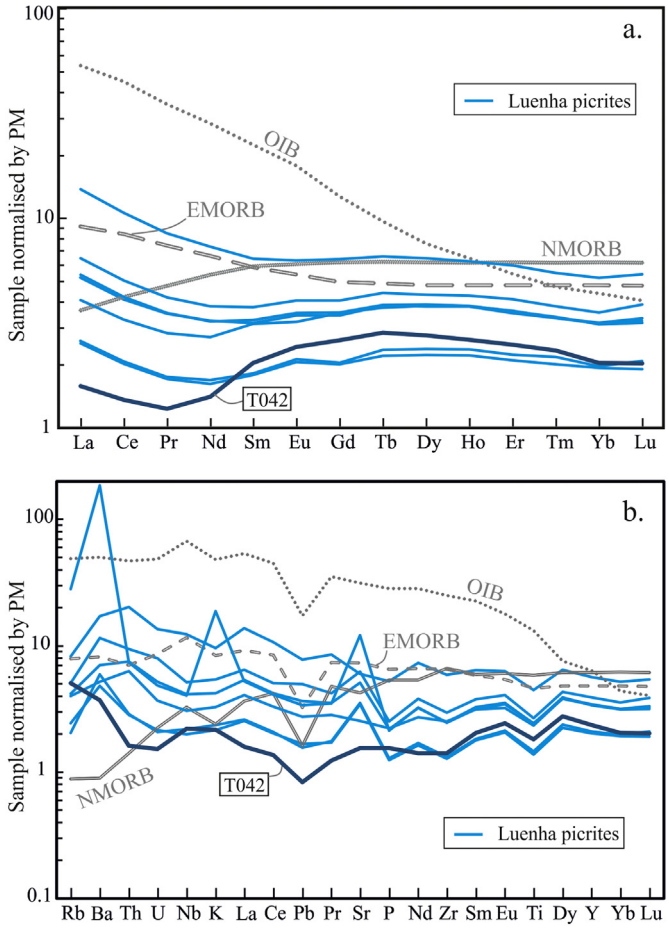

Fig. 6. Primitive mantle -normalized a) REE and b) incompatible element patterns of the Luenha picrites. Compositions of average OIB (ocean iceland basalt), NMORB (normal MORB), and EMORB (enriched MORB) from Sun and McDonough (1989) are shown for comparison. Normalization is after Sun and McDonough (1989).

6. Estimating the parental and primary melts

In this section we examine the geochemical effects of secondary alteration, phenocryst accumulation, and fractional crystallization and estimate the parental and primary melt compositions.

6.1. Secondary alteration

All of the Luenha picrite samples show some indications of secondary alteration, although most of them are exceptionally well-preserved for olivine-bearing lavas of the Karoo LIP. Previous studies of variably altered CFBs suggest that the influence of alteration is largely limited to fluid-mobile large-ion lithophile elements (LILE) such as Rb, K, Ba, and possibly Sr, whereas REE (and Nd isotopic compositions) are not significantly affected (e.g. Fleming et al., 1992; Luttinen and Furnes, 2000). The petrographically most strongly altered sample T026B (LOI ~ 5 wt%) shows strong selective LILE-enrichment. We regard that secondary alteration has considerably affected the LILE in this sample and note that the exceptionally high initial $^{87}Sr/^{86}Sr$ may have been influenced as well. The other Luenha River samples (T026C–G) are moderately altered. They show variably high initial $^{87}Sr/^{86}Sr$, and some exhibit mild selective enrichment in LILE. We cannot rule out some effect of secondary alteration on LILEs and $^{87}Sr/^{86}Sr$ in their case, but consider crustal contamination to be mainly responsible for producing their geochemical signatures (Section 6.3.). In contrast, samples T039 and T042 are petrographically weakly altered and have chondrite-like initial $^{87}Sr/^{86}Sr$. Sample T039 lacks indications of LILE-enrichment. Sample T042 shows mild enrichment of Ba and Rb relative to Th. Overall, we consider that the geochemical compositions of T039 and T042 are likely to correspond to magma compositions rather well

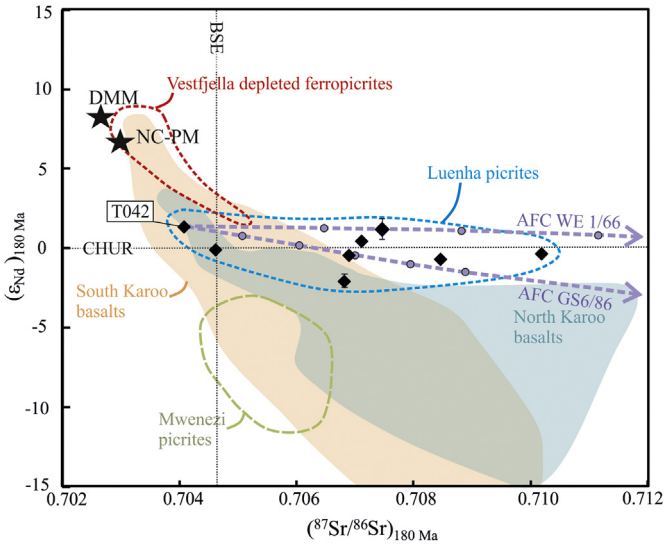

Fig. 7. Initial Nd and Sr isotopic compositions of the Luenha picrites. Compositions of the North Karoo and South Karoo flood basalts (compilation from Luttinen, 2018), Mwenezi picrites (Ellam and Cox, 1989), and Vestfjella depleted ferropicrites (Heinonen et al., 2010) are shown for comparison. DMM (depleted MORB mantle; Workman and Hart, 2005) and NC-PM (non-chondritic primitive mantle; Jackson and Jellinek, 2013) show compositions of potential mantle sources. The results of crustal contamination modeling (Supplementary Table S3) using two assimilants are indicated by dotted arrows (AFC WE1/66, Eglington and Armstrong, 2003; AFC GS6/86 Moyes et al., 1995). Purple dots indicate 1% steps of contamination (up to 5 wt%) relative to original melt mass. CHUR (chondritic uniform reservoir) composition is from Jacobsen and Wasserburg, 1980 and BSE (bulk silicate Earth) from Caro and Bourdon, 2010. Analytical 2σ errors for the Luenha picrite data are indicated when larger than the plot symbol. (For interpretation of the references to colour in this figure legend, the reader is referred to the web version of this article.)

also in the case of LILE. Possible mobility of Rb is likely to have occurred soon after the lava eruption and the initial $^{87}Sr/^{86}Sr$ values of these samples are also likely to correspond to magmatic compositions.

6.2. Accumulation and fractional crystallization

Strong control of MgO on the major element trends and compatible behavior of Ni and Cr suggest fractionation or accumulation of olivine (and minor spinel) in the evolution of the Luenha picrite magmas. The presence of unaltered olivine phenocrysts in samples T026E, T026F, T026G, T039, and T042 allows distinction between olivine accumulation and fractional crystallization using Mg-Fe equilibrium between olivine and melt. In order to constrain the compositions of magmas prior to olivine accumulation or fractionation, we calculated equilibrium melt compositions using K_D values of 0.3 and 0.35 for the olivine-melt Mg-Fe exchange reaction to allow for composition-dependence of the K_D value (Herzberg and O'Hara, 2002). To constrain the oxidation state of the parental melts, we measured the compositions of spinel cores from the primitive (olivine up to $Fo_{88.9}$) flow top sample T026E. Because of rapid cooling, post-crystallization re-equilibration is unlikely, and we consider that the spinels in this sample record the oxidation conditions. The melt Fe^{2+}/Fe_{tot} in equilibrium with the averaged and stoichiometrically corrected spinel compositions is 0.9 according to the experimentally constructed equation of Maurel and Maurel (1982). This value was used in all parental melt calculations. We consider that possible accumulation of volumetrically minor plagioclase and Cr-spinel has had a negligible effect on the major element compositions and we did not include these phases in the calculations.

Examination of the data shows that the observed variations in the whole-rock geochemistry of the Luenha picrite series are mainly caused by olivine accumulation. Most of the high-Mg samples are typified by less magnesian olivine than what would be in equilibrium with the whole rock (Supplementary Fig. S3). We have corrected for the geochemical effects of olivine accumulation in these samples by assuming that the bulk composition of the accumulated olivine is similar to the average of the measured core compositions, and by subtracting such olivine from the whole-rock composition until the recalculated whole-rock and the average olivine are in Mg-Fe equilibrium.

The picritic sample T039 (MgO = 17 wt%) has considerably more Fe-rich olivine (average Fo_{78}) than the other samples. In addition, the olivine cumulate samples T026F and T026G (MgO = 24–25 wt%) are typified by compositionally variable olivine populations ($Fo_{83–87}$) with relatively low-Mg average compositions ($Fo_{85–86}$), which would indicate basaltic parental magmas for them. Since we are mainly interested in the most primitive magma compositions, we excluded these samples from the equilibrium calculations.

The basaltic sample T026E (MgO = 9 wt%) and the olivine cumulate sample T042 (MgO = 27 wt%) have quite similar and uniformly Mg-rich olivine compositions. We examined the equilibrium in these samples using $K_D(Mg\text{-}Fe)_{ol–liq}$ of both 0.3 and 0.35 that are compatible with variably MgO-rich melts. The high-Mg olivine in the basaltic sample T026E indicates that some olivine phenocrysts have been physically separated from the erupted magma (i.e. accumulated elsewhere). Addition of average olivine (Fo_{88}) yields picritic accumulation-corrected melts with MgO = 12.4–14.6 wt% (Table 3) for this sample. In contrast, sample T042 shows indications of olivine accumulation. Accumulation correction using the average olivine (Fo_{87}) yields recalculated equilibrium compositions which straddle the basalt-picrite boundary (Le Bas, 2000) at MgO = 10.5–12.3 wt%.

In the case of samples T026E and T042, we also calculated parental melt compositions that are in equilibrium with the most magnesian olivine phenocrysts found in the rocks (Fo_{89}). We calculated the parental melt of such olivine phenocrysts by adding equilibrium olivine to

Table 3
Compositions of accumulation-corrected, parental, and primary melts for selected Luenha picrites, and calculated temperatures for the primary melts.

Sample name	Equilibrium olivine (Fo-%)	$K_D^{ol\text{-}liquid}$	Addition or subtraction[a]	Temperature (°C)	SiO_2	TiO_2	Al_2O_3	FeO_{TOT}	MnO	MgO	CaO	Na_2O	K_2O	P_2O_5
Accumulation corrected melts														
AL-T026E	87.3[c]	0.3	+7.7		47.92	0.90	13.53	11.92	0.18	12.36	10.94	1.88	0.27	0.11
AL-T026E	87.3[c]	0.35	+13.5		47.40	0.84	12.68	11.95	0.18	14.56	10.27	1.76	0.25	0.10
AL-T042	87.3[c]	0.3	−48.0		48.02	0.74	15.78	10.03	0.15	10.47	13.07	1.55	0.13	0.07
AL-T042	87.3[c]	0.35	−45.2		47.66	0.70	14.98	10.13	0.15	12.31	12.42	1.48	0.12	0.06
AL-T042[e]	87.3[c]	0.34	−45.8		47.73	0.71	15.14	10.11	0.15	11.93	12.55	1.49	0.12	0.06
Parental melts					SiO_2	TiO_2	Al_2O_3	FeO_{TOT}	MnO	MgO	CaO	Na_2O	K_2O	P_2O_5
AL-T026E	88.9[d]	0.3	+7.0		47.42	0.84	12.61	11.89	0.17	14.77	10.20	1.75	0.25	0.10
AL-T026E	88.9[d]	0.35	+16.0		46.81	0.76	11.52	11.96	0.15	17.56	9.32	1.60	0.23	0.09
AL-T042	88.6[d]	0.3	+4.0		47.73	0.71	15.16	10.10	0.14	11.93	12.56	1.49	0.12	0.06
AL-T042	88.6[d]	0.35	+5.4		47.28	0.66	14.19	10.22	0.14	14.18	11.76	1.40	0.11	0.06
AL-T042[e]	88.6[d]	0.34	+5.0		47.38	0.67	14.40	10.19	0.14	13.68	11.94	1.42	0.11	0.06
Primary melts					SiO_2	TiO_2	Al_2O_3	FeO_{TOT}	MnO	MgO	CaO	Na_2O	K_2O	P_2O_5
AL-T042	89	0.3	+5.5	1445[b]	47.59	0.69	14.86	10.12	0.14	12.66	12.31	1.46	0.12	0.06
AL-T042	92	0.3	+20.6	1529[b]	46.66	0.60	12.78	9.98	0.12	17.87	10.58	1.26	0.10	0.05
AL-T042	89	0.35	+7.0	1491[b]	47.15	0.65	13.91	10.23	0.14	14.86	11.53	1.37	0.11	0.06
AL-T042	92	0.35	+26.0	1582[b]	46.08	0.54	11.49	10.05	0.11	20.94	9.53	1.13	0.09	0.05
AL-T042[e]	91	0.34	+17.5	1532[b]	46.61	0.59	12.70	10.16	0.12	17.87	10.53	1.25	0.10	0.05
Melting experiments[f]					SiO_2	TiO_2	Al_2O_3	FeO_{TOT}	MnO	MgO	CaO	Na_2O	K_2O	P_2O_5
KR-4003 (3GPa, F = 19%)	91	0.35		1530	47.04	0.71	13.17	8.82	0.18	17.72	11.01	0.94	0.41	–
KR-4003 (3 GPa, F = 24%)	91	0.36		1540	47.25	0.64	12.55	8.92	0.17	18.35	10.94	0.83	0.34	–
KR-4003 (4 GPa, F = 13%)	90	0.35		1610	46.00	1.28	10.46	10.76	0.19	20.10	9.41	1.09	0.71	–
KR-4003 (4 GPa, F = 39%)	92	0.36		1660	46.80	0.47	10.42	9.80	0.19	22.61	9.08	0.41	0.22	–

Units for oxide concentrations are wt%. Normalized on a volatile-free basis to 100%.

[a] The required amount of added (+) or subtracted (−) olivine to reach equilibrium between olivine and melt.

[b] Calculated using melt-olivine equilibrium thermometer (eq. 4) of Putirka et al. (2007) when P = 3.5 GPa and water content 1 wt%.

[c] The composition of average olivine core in the sample.

[d] The composition of the most forsteritic olivine core in the sample.

[e] Preferred model calculated based on constraints from melting experiments of Walter (1998).

[f] Fertile mantle primary melt compositions based on melting experiments of pyrolitic fertile peridotite KR-4003 (Walter, 1998). Temperatures refer to experiment conditions. F = Degree of melting.

the accumulation-corrected compositions in 1 wt% steps until the equilibrium olivine reached Fo_{89} (Table 3). These parental melt compositions for samples T026E and T042 are low-Ti picrites with MgO = 11.9–17.6 wt%.

6.3. Crustal contamination

Whereas crystal-liquid fractionation processes can account for the overall major and trace element variations in the Luenha picrites, they cannot explain the wide ranges of incompatible trace element ratios and especially the variation in initial isotopic compositions. Most of the Luenha picrites show high PM-normalized $(Th/Nb)_N$ (1.3–2.1) and $(La/Nb)_N$ (1.1–1.3) values and initial $^{87}Sr/^{86}Sr$ typical of crustally contaminated Karoo picrites (Figs. 6–7, e.g., Riley et al., 2005; Luttinen et al., 2015; Heinonen et al., 2016). We consider that, unlike the other Luenha picrites, sample T042 has not been significantly influenced by crustal contamination because of its PM-like isotopic composition and incompatible trace element ratios (Fig. 6b), including low $(Th/Nb)_N$ (0.73) and $(La/Nb)_N$ (0.72).

We estimate the effect of crustal contamination on the other Luenha samples by using the assimilation and fractional crystallization (AFC) equations of DePaolo (1981). The parameters used for the AFC modeling are listed in Supplementary Table S3. Our model uses the estimated parental melt of T042 as the starting composition. The isotopic compositions of the Luenha picrites call for an upper crustal contaminant with notably radiogenic initial $^{87}Sr/^{86}Sr$ but nearly chondritic initial ε_{Nd}, i.e. different from crustal contaminants of most Karoo CFBs (Fig. 7). Two models using a Namaqua-Natal biotite gneiss sample WE 1/66 (Eglington and Armstrong, 2003) and a sedimentary rock sample GS6/86 from Ahlmanryggen-Borgmassivet area, Antarctica (Moyes et al., 1995), as contaminants serve to illustrate that fractional crystallization and crustal contamination may be responsible for the overall compositional variability in the Luenha picrites (Fig. 7). The amount of crustal contamination suggested by the AFC models is in the order of 1–6 wt% Bearing in mind that real contaminants would probably have been incompatible element-enriched partial melts rather than bulk wallrock (see Bohrson and Spera, 2001; Heinonen et al., 2016), the amounts of crustal material in the model may be overestimated.

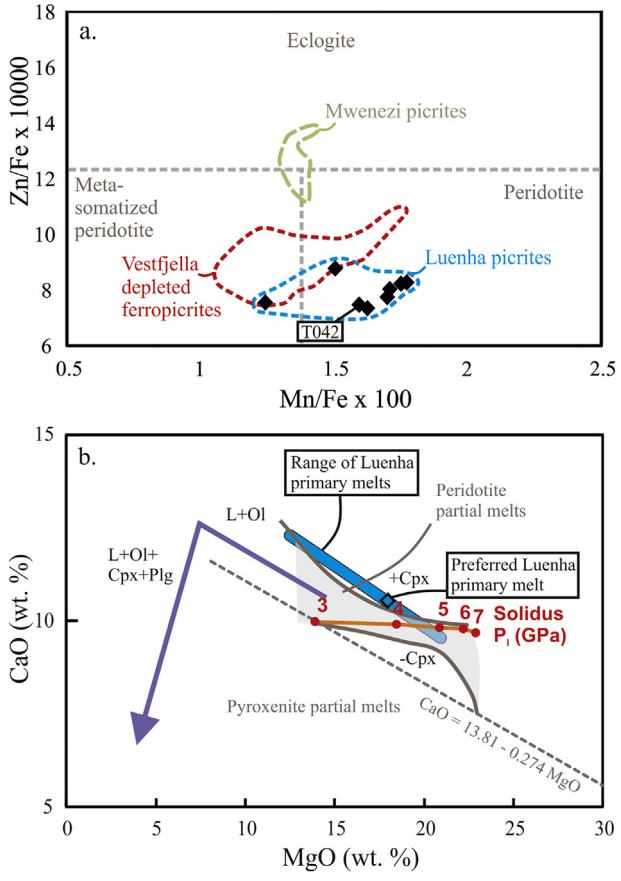

Fig. 8. a) 10000*Zn/Fe vs. 100*Mn/Fe and b) CaO vs. MgO variation diagrams for the Luenha picrites. In a), compositions of the Luenha picrites (sample T042 highlighted), Mwenezi picrites (Ellam and Cox, 1989), and Vestfjella depleted ferropicrites (Heinonen and Luttinen, 2008) are plotted in the mantle residue diagram of Le Roux et al. (2011). In b), the blue line indicates primary melt compositions for the Luenha picrite T042 in the pyroxenite and fertile peridotite partial melt diagram of Herzberg and Asimow (2008). The primary melts were calculated assuming Fe^{2+}/FeO_{tot} of 0.9, K_D of 0.3 and 0.35, and equilibrium with Fo_{89} and Fo_{92} olivine in the mantle residue (Table 3). The preferred model for primary melt (residual olivine Fo_{91}, and $K_D = 0.34$) is indicated with blue diamond. The grey field represents primary fertile peridotite partial melts, whereas peridotite partial melt compositions affected by accumulation or removal of clinopyroxene are indicated with +Cpx and -Cpx, respectively. Near-solidus compositions of primary peridotite partial melts at different pressures are shown in red. The purple arrow illustrates liquid line of descent for successive fractional crystallization of olivine (L + Ol) and olivine, clinopyroxene, and plagioclase (L + Ol + Cpx + Plg). (For interpretation of the references to colour in this figure legend, the reader is referred to the web version of this article.)

6.4. Primary melts

Estimation of primary melt compositions can help to constrain the mantle source composition and melting conditions. Primary melts of peridotite are generally regarded to be in equilibrium with high-Mg residual olivine of $Fo_{90–92}$ (e.g., Albarede, 1992), although a wider range of residual olivine compositions of $Fo_{89–93}$ may also be realistic (e.g., Green and Falloon, 1998; Thompson and Gibson, 2000). We have calculated a set of theoretical primary melt compositions for the Luenha picrites on the basis of the most primitive sample T042 by adding equilibrium olivine to the accumulation-corrected melts (Table 3) in 1 wt% steps until the recalculated melt is in equilibrium with mantle residual olivine Fo_{89} and Fo_{92}. We consider that more magnesian residual olivine compositions are not supported by the PM-like geochemical features of the Luenha picrites. Using these two mantle olivine end-member compositions and two $K_D(Fe\text{-}Mg)_{ol\text{-}liq}$ values of 0.3 and 0.35, we have obtained four picritic primary melt compositions (MgO = 12.7–20.9 wt

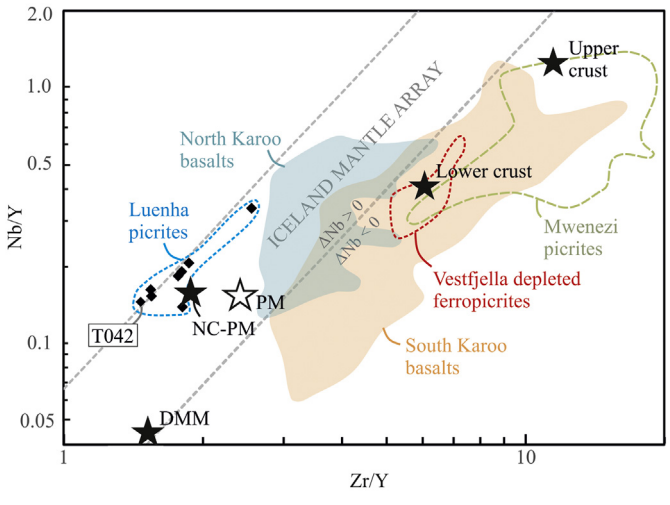

Fig. 9. Nb/Y vs. Zr/Y variation diagram for the Luenha picrites. Compositions of the North Karoo and South Karoo flood basalts (compilation from Luttinen, 2018), Vestfjella depleted ferropicrites (Heinonen and Luttinen, 2008), and Mwenezi picrites (Ellam and Cox, 1989) are shown for comparison. DMM (depleted MORB mantle; Workman and Hart, 2005), PM (primitive mantle; Sun and McDonough, 1989), and NC-PM (non-chondritic primitive mantle; Jackson and Jellinek, 2013) show compositions of potential mantle sources. Average upper and lower crust compositions are from Wedepohl (1995). The Iceland mantle array is from Fitton et al. (1997). $\Delta Nb = 1.74 + \log(Nb/Y) - 1.92 \log(Zr/Y)$ (Fitton et al., 1997).

%) that are likely to bracket the overall range of feasible primary melt compositions.

Comparison between the modeled primary melts and experimentally derived melts of fertile "pyrolitic" lherzolite (Walter, 1998) indicates that the experimental melts have low-Ti picritic compositions quite similar to our modeled primary melts at ca. 20% of melting and 3–4 GPa pressure and that they are in equilibrium with residual olivine Fo_{91} (Table 3). According to Herzberg and O'Hara (2002), the Fe-Mg equilibrium between olivine and such melts has relatively high K_D values of 0.34–0.35. We have utilised these constraints in calculation of a set of 'preferred melt models' using the observed Fe^{2+}/Fe^{tot} of =0.9, $K_D(Fe\text{-}Mg)_{ol\text{-}liq}$ of 0.34, and mantle residual olivine Fo_{91} (Table 3). Our preferred primary melt model for sample T042 has MgO of 17.9 wt% and we regard it to represent a conservative estimate of the primary melts of the Luenha picrites.

7. Mantle sources and melting conditions

In this section, we constrain the mineral composition, geochemical character, and temperature of the mantle source of the Luenha picrites on the basis of their geochemistry and estimated primary melt compositions. Finally, we discuss the implications of our results in the context of Karoo LIP, global mantle reservoirs, and plume hypothesis.

7.1. Mantle source characteristics

The mildly depleted initial Nd isotopic composition of the uncontaminated sample T042 ($\varepsilon_{Nd} = +1.4$) sets the Luenha source apart from the previously identified enriched and depleted mantle sources of Karoo picrites and flood basalts (Fig. 7). In the case of the Luenha picrites, the precision of Ni and Mn data for olivine phenocrysts (Sobolev et al., 2007; cf. Matzen et al., 2017) is not sufficient for evaluation of the mineral composition of the source (Supplementary Table S2). Whole-rock tracers of mantle source mineralogy, however, consistently point to a dominantly peridotitic source for the Luenha picrites: in the Mn/Fe vs. Zn/Fe plot the Luenha picrites cluster within the field of a peridotitic residue (Le Roux et al., 2011) (Fig. 8a) and the modeled primary melts (Table 3) have high CaO values at a given MgO typical of peridotite-derived melts (Herzberg and Asimow, 2008) (Fig. 8b).

The unique character of the Luenha picrites among Karoo picrites is underlined by their Nb-Zr-Y systematics. Whereas Nb/Y and Zr/Y show coupled variation during partial melting of mantle, notable variability in Nb/Y at given Zr/Y is a strong indicator of mantle heterogeneity and can be quantified using the ΔNb parameter of Fitton et al. (1997). In a Zr/Y vs. Nb/Y diagram (Fig. 9), the Luenha picrites have notably high Nb/Y despite their low Zr/Y (i.e. positive ΔNb). They plot relatively close to PM and cluster along the upper limit of the so-called Icelandic mantle plume array of Fitton et al. (1997). With regard to the Nb-Zr-Y ratios, the Luenha picrites and their mantle source therefore exhibit high-ΔNb (Nb-undepleted) compositions typical of many plume-related magma suites (Fitton, 2007). In contrast, both the enriched Mwenezi picrites and the depleted Vestfjella ferropicrites plot below the Icelandic plume array within the field of Nb-depleted compositions. We consider that the source of the Luenha picrites must have resided in the convectice mantle because of the thermodynamic arguments against production of low-Ti tholeiites by melting of SCLM (Arndt and Christensen, 1992) and the Nb-depleted compositions typically associated with lamproites and other presumably SCLM-sourced enriched magma types (Gibson et al., 1995; Fitton, 2007).

Bearing in mind that many picrites, if not most, are hybrids of magmas derived from compositionally different parts in the mantle (Sobolev and Shimizu, 1993; Maclennan, 2008), it is possible that the Luenha picrites record a specific high-ΔNb mantle reservoir or mixing of magmas from relatively Nb-depleted and Nb-enriched sources. Evidence of global mantle reservoirs with elevated ΔNb is recorded in hotspot-related enriched MORB and OIB (Fitton, 2007) and mainly relate to the EM1 (enriched mantle 1), EM2 (enriched mantle 2), and HIMU (high-μ mantle) components of Zindler and Hart (1986). Only HIMU-affinity magmas frequently show overlap with the Luenha picrites with regard to ΔNb (Fig. 10), however, and notably low U/Pb (<0.2) in the uncontaminated sample T042 is inconsistent with a significant HIMU mantle or magma component (U/Pb ~0.4–0.7; Willbold and Stracke, 2010; Hanyu et al., 2011). Accordingly, we maintain that mixing of DM-, EM1-, EM2- and HIMU-like mantle sources or magmas is an unlikely petrogenetic scenario for the Luenha picrites (Fig. 10).

Importantly, isotopically depleted, but otherwise PM-like (e.g. high-ΔNb and low-U/Pb) components may also be important mantle reservoirs: The coupling of depleted Nd and Sr isotopic compositions with high $^3He/^4He$ in several OIB suites is suggestive of distinctive, moderately depleted mantle components (e.g. Zindler and Hart, 1986). Recently, such components have been regarded by many to include a category of ancient, isotopically non-chondritic reservoirs which formed as residues of rapid melt extraction soon after the formation of Earth's core (e.g. Boyet and Carlson, 2006; Tolstikhin and Hofmann, 2005). Despite moderate depletion in highly incompatible elements relative to chondritic PM, the purported non-chondritic primitive mantle reservoirs may still be chemically quite similar to fertile PM peridotite (Jackson et al., 2010; Jackson and Carlson, 2011; Jackson and Jellinek, 2013). The strongest evidence for non-chondritic primitive mantle reservoirs has been found in LIPs (Ontong-Java, Caribbean-Colombian and North Atlantic igneous provinces; Jackson and Carlson, 2011; Jackson et al., 2010). The incompatible trace element ratios of the most primitive Luenha picrite are nearly identical to those suggested for the non-chondritic primitive source (Fig. 11) and the ΔNb values are indistinguishable within analytical precision (ca. ±0.1; see Section 3.2.) (Fig. 10). The initial Nd and Sr isotopic compositions of the Luenha source (initial $\varepsilon_{Nd} + 1.4$; $^{87}Sr/^{86}Sr$ 0.7041), however, are slightly less depleted than the currently estimated composition of the non-chondritic

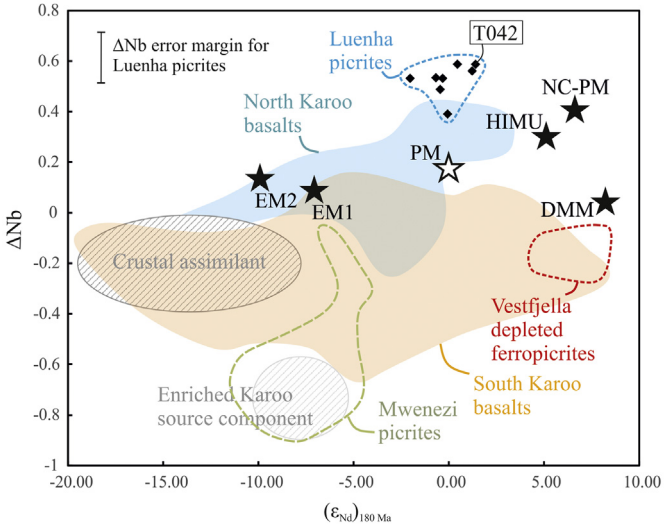

Fig. 10. ΔNb vs. initial εNd (180 Ma) variation diagram for the Luenha picrites. Compositions of the North Karoo and South Karoo flood basalts (compilation from Luttinen, 2018), Mwenezi picrites (Ellam and Cox, 1989), and Vestfjella depleted ferropicrites (Heinonen et al., 2010; Heinonen and Luttinen, 2008) are shown for comparison. DMM (depleted MORB mantle; Workman and Hart, 2005), PM (primitive mantle; Sun and McDonough, 1989; Jacobsen and Wasserburg, 1980), NC-PM (non-chondritic primitive mantle; Jackson and Jellinek, 2013), EM1, and EM2, and HIMU (enriched mantle 1 and 2; high μ mantle; not calculated to 180 Ma due to uncertain concentrations; Zindler and Hart, 1986; Fitton, 2007) represent potential mantle sources. Compositions of plausible mantle sources of the enriched Mwenezi picrites (Enriched Karoo source component) and crustal assimilants are illustrated. ΔNb = 1.74 + log (Nb/Y) – 1.92 log (Zr/Y) (Fitton et al., 1997).

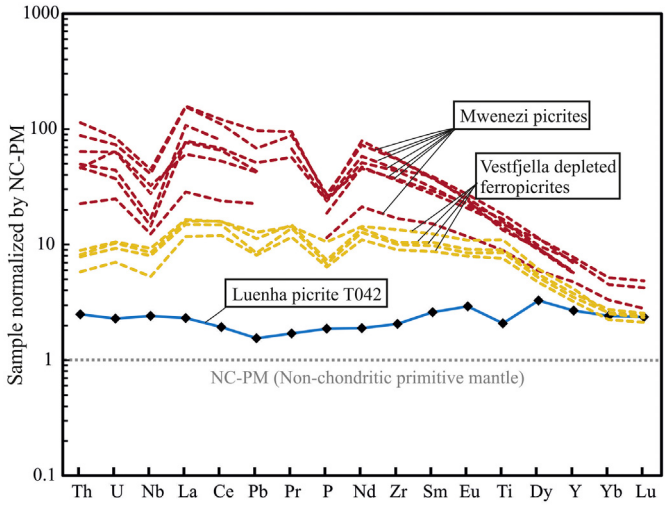

Fig. 11. Non-chondritic primitive mantle (NC-PM; Jackson and Jellinek, 2013) -normalized incompatible element pattern of Luenha picrite T042. Compositions of the Mwenezi picrites (Ellam and Cox, 1989) and Vestfjella depleted ferropicrites (Heinonen and Luttinen, 2008) are shown for comparison.

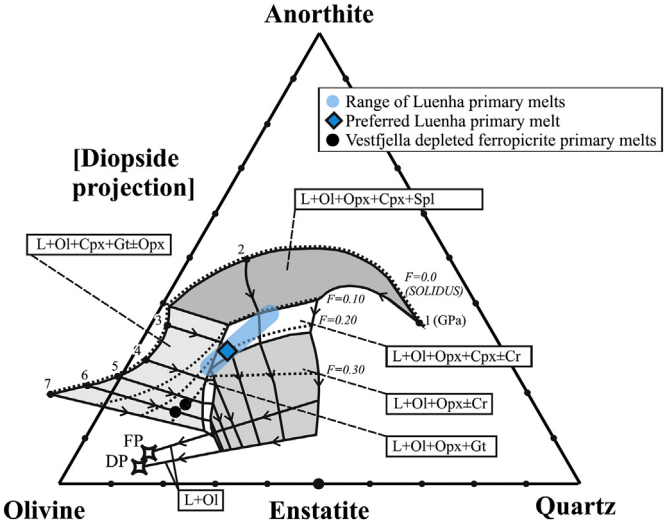

Fig. 12. Comparison between the compositions (mol. %) of Luenha primary melts (sample T042) and liquids in equilibrium with mantle peridotite in the projection from diopside, $Na_2O{\cdot}Si_3O_6$, and $K_2O{\cdot}Si_3O_6$ into the plane olivine–anorthite–silica of Herzberg and O'Hara (2002) and Herzberg et al. (2007). FP is fertile peridotite and DP is depleted peridotite. Dotted lines indicate equal fractions of melting (F). Solid arrow lines indicate cotectic equilibria at 1–7 GPa pressures towards increasing temperature. Mantle peridotite phase assemblages in equilibrium with melt in each field are indicated (L = liquid, Ol = olivine, Opx = orthopyroxene, Cpx = clinopyroxene, Gt = garnet, Spl = spinel and Cr = chromite). The field of Luenha primary melts (sample T042) have been calculated assuming Fe^{2+}/FeO_{tot} of 0.9, K_D of 0.3 or 0.35 and equilibrium with Fo_{89} or Fo_{92} olivine in the mantle residue (Table 3). The preferred model for Luenha primary melt (K_D of 0.34 and residual olivine Fo_{91}) is indicated with blue diamond. The estimated primary melts for the Vestfjella depleted ferropicrites (Heinonen and Luttinen, 2010) are shown for comparison. (For interpretation of the references to colour in this figure legend, the reader is referred to the web version of this article.)

reservoirs (initial ε_{Nd} + 5 to +9, $^{87}Sr/^{86}Sr$ 0.7026 to 0.7034; Jackson and Jellinek, 2013). (Fig. 7)

We regard that among the major global mantle reservoirs, the non-chondritic primitive mantle is the most plausible principal source component for the Luenha picrites and that relatively low ε_{Nd} could indicate presence of a minor LREE-enriched component in the Luenha source (Fig. 10). Mixing of melts derived from such moderately depleted and enriched parts of mantle in the magma plumbing system could help to explain the S-shaped REE-pattern, i.e. enrichment of La and Ce relative to other light REE, detected in the most primitive Luenha picrite (Fig. 6a). Given that the incompatible element and isotopic compositions of the various suggested mantle reservoirs are not precisely defined, we consider it is theoretically also possible that the Luenha picrites could record a mildly depleted, i.e. nearly chondritic, variant of non-chondritic primitive mantle reservoirs, although the consistency of depleted $^{142}Nd/^{144}Nd$ in terrestrial rocks does not support survival of nearly chondritic primordial reservoirs in the mantle (Boyet and Carlson, 2006). We conclude that the mantle source of the Luenha picrites was mainly peridotitic and had a broadly PM-like bulk composition on the scale of primary melt extraction.

7.2. Melting conditions

The residual mineral composition and conditions of mantle melting can be estimated using the CMAS normative phase diagrams for peridotitic mantle presented by Herzberg and O'Hara (2002) and Herzberg et al. (2007) (Fig. 12). The overall compositional range of our primary melt models expresses the potential influence of uncertain Fe-Mg partitioning and residual olivine compositions on the mantle restite and melting conditions and the preferred model is considered to yield the best estimate (Table 3; Section 6.4.). In the diopside projection of the CMAS diagram for fertile lherzolite, which closely corresponds to estimated primitive upper mantle (Herzberg and O'Hara, 2002), the compositions of the modeled primary melts of the Luenha picrites are suggestive of 1.5–4 GPa pressure for melt extraction, a lherzolitic residue, and ca. 10–25% of partial melting (Fig. 12). It is noteworthy that the modeled primary melts plot mainly within the field of garnet-free residue and that total consumption of garnet in the source would explain the flat PM-normalized REE patterns (Fig. 6a) and high concentrations of garnet-compatible Cr (Pertermann et al., 2004; Table 1) and Al in the Luenha picrites. This Al-enrichment is also recorded in the magmatic spinels (see Kamenetsky et al., 2001; Supplementary Table S2).

Comparison between the preferred primary melt model and experimental data in the CaO vs. MgO plot (Fig. 8b), CMAS-projection (Fig. 12), and Table 3 points to generation of the Luenha picrites at ca. 3–4 GPa pressure and 20% of partial melting. We regard these values may provide a rough estimate of the average pressure conditions and degree of melting during formation of the primary melts of the Luenha picrites.

The modeled primary melts can be also applied to estimation of liquidus temperatures using the equations of Putirka et al. (2007). Assuming H_2O/Ce of ≤200 typical of oceanic basalts (Michael, 1995), we regard the amount of water in the primary melts to be ≤1 wt%. Using primary H_2O contents of 1 wt.%, the liquidus temperatures calculated for the modeled melts based on melt and equilibrium olivine compositions at 3.5 GPa (Putirka et al., 2007) show a range of ca. 1445–1582 °C, and 1532 °C for our preferred model (Table 3).

7.3. The Luenha picrites and the North Karoo CFBs

The evaluation of the province-scale role of the Luenha picrites is critically dependent on their genetic relationship with the Karoo CFBs. Significantly, it seems that the Luenha picrites and the voluminous and rapidly emplaced North Karoo CFBs were derived from a similar PM-like mantle source.

We claim that, based on just their low-Ti and high-ΔNb compositions, the Luenha picrites represent the only presently known geochemically plausible parental magma type for the low-Ti CFBs of North Karoo (Figs. 4 and 10). Both the Luenha picrites and the North Karoo CFBs also have low Sm/Yb values (mainly <1.6; dataset of Luttinen, 2018) suggestive of similar mantle compositions and high-degree melting conditions. The other reported Karoo picrites and South Karoo CFBs have more varied and mostly higher Sm/Yb (mainly >1.6; dataset of Luttinen, 2018). Furthermore, the Luenha picrites and the least-

contaminated North Karoo CFBs exhibit PM-like initial Nd and Sr isotopic compositions (Fig. 7). Relatively low ΔNb and ε_{Nd} in most North Karoo magmas are readily ascribed to crustal contamination of Luenha-like parental magmas. The variability in ΔNb and ε_{Nd} displayed by the Luenha picrites and the least-contaminated North Karoo CFBs may relate to different amounts of subordinate enriched and depleted components in a mildly heterogeneous, possibly non-chondritic, PM-like mantle source (Fig. 10).

Given that the Luenha picrites (180 Ma ≤) are also geographically and stratigraphically associated with North Karoo CFBs (Fig. 3), we regard these similarities to suggest a plausible parent-daughter relationship between the Luenha picrites and the North Karoo CFBs. The high volume of North Karoo CFBs suggests that their source was a significant component in the Karoo LIP.

7.4. A plume in the Karoo LIP?

It is widely accepted that mantle plumes bring up material from the deep mantle (e.g. French and Romanowicz, 2015). Several authors have suggested that the assumed non-chondritic primitive mantle reservoir may be an important component in mantle plumes: this reservoir is envisaged to reside below the 660 km discontinuity (Boyet et al., 2003), possibly within the large low shear-velocity provinces (LLSVPs) of deep mantle (Jackson and Carlson, 2011). Given that many Phanerozoic LIPs have formed along the rims of LLSVPs (e.g. Torsvik et al., 2010), non-chondritic mantle reservoirs could be significant magma sources of LIPs (Jackson and Carlson, 2011).

In the case of the Karoo LIP, the possible role of a mantle plume has been a recurrent topic of discussion (Burke and Dewey, 1973; Hastie et al., 2014; Storey, 1995; White, 1997). Key evidence for plume-derived Karoo magmatism include indications of high mantle temperatures (Campbell and Griffiths, 1990) and rapid production of large melt volumes (Svensen et al., 2012). However, the notably high temperatures inferred from the picrites have alternativaly been explained by heating of the mantle underneath the Gondwana supercontinent (Coltice et al., 2007; Heinonen et al., 2015) largely because the sources of the previously reported depleted and enriched picrite types in the Karoo LIP have been interpreted to reside in the upper mantle rather than in deep-seated mantle plumes (Ellam, 2006; Ellam and Cox, 1989, 1991; Harris et al., 2015; Heinonen et al., 2010, 2016; Heinonen and Kurz, 2015; Kamenetsky et al., 2017; Luttinen et al., 2015; Sweeney et al., 1991). In contrast, our results on the Luenha picrites indicate a previously unknown high-temperature mantle source component which also shows geochemical similarities to PM-like components associated with OIB and oceanic plateaux. Importantly, the Luenha picrites also show affinity to the rapidly produced North Karoo CFBs that formed largely above the sub-African LLSVP (Luttinen, 2018).

We conclude that the simplest explanation for the diagnostic primary features of the Luenha picrites is high degree partial melting of a mildly depleted, but otherwise PM-like plume source. Geochemically, this source was quite similar to the postulated non-chondritic primitive reservoir. If the Luenha picrites represent the principal source of the voluminous North Karoo CFBs, possibly more than half of the Karoo LIP may have been derived from a mantle plume. A significant plume source in North Karoo would help to explain the physical and geochemical manifestations of plume activity, such as triple junctions, aulacogens, paleo flow indications in sediments and magmatic flow directions (Burke and Dewey, 1973; Cox, 1988; Hastie et al., 2014; cf. Jourdan et al., 2006), as well as the rapid emplacement of the North Karoo CFBs (Svensen et al., 2012) and indications of exceptionally high mantle potential temperatures in the upper mantle-sourced South Karoo picrites (Heinonen et al., 2015). The Luenha picrites may thus represent the first discovery of a plume-derived picrite suite in the Karoo LIP.

8. Conclusions

1. We report a previously undocumented suite of Karoo-related olivine-rich lavas (Luenha picrites) from the eastern flank of the Moatize-Luia graben, Central Mozambique.
2. Based on magnesian olivine (up to Fo_{89}) and whole rock compositions and geochemical modeling, the Luenha picrites were derived from highly magnesian primary melts (MgO = 13–21 wt%; preferred model MgO = 18 wt%).
3. The Luenha picrite suite includes a fresh sample (T042) that lacks geochemical indications of crustal contamination. The compositional variations in the picrite suite can largely be explained by fractionational crystallization and contamination of T042-like parental melts by crustal material and subsequent accumulation of olivine.
4. Geochemical data on sample T042 facilitate estimation of the primary melt and mantle source compositions. The Luenha picrite series was derived from a peridotitic, PM-like mantle source, and the preferred primary melt indicates a liquidus temperature of ca. 1530 °C.
5. Geochemical similarities, specifically low TiO_2 contents, positive ΔNb values, flat heavy REE patterns, and mildly depleted Sr and Nd isotopic compositions, support a similar mantle source for the Luenha picrites and the voluminous low-Ti CFBs of the North Karoo subprovince. The same features distinguish the Luenha picrites from the previously reported picrites of the South Karoo subprovince.
6. We propose that the mantle source of the Luenha picrites, and, by inference, the source of voluminous North Karoo CFBs, records a PM-like reservoir resembling recently proposed non-chondritic mantle plume sources. The Luenha picrites may thus provide the first direct geochemical sample of a significant mantle plume source component for the Karoo LIP.

Supplementary data to this article can be found online at https://doi.org/10.1016/j.lithos.2019.105152.

Acknowledgements

We thank Nicholas Arndt, Vadim Kamenetsky, and editor Andrew Kerr for their helpful comments. We also wish to thank António Alface, Estêvão Sumburane, and Teofilo Gove for their help during the field operations. The contributions of Hannu Huhma, Arto Pulkkinen, and Leena Järvinen of the Geological Survey of Finland, Radoslaw Michallik and Pasi Heikkilä from the University of Helsinki, Charles Knaack and Ashley Steiner from the Washington State University and Richard W. Carlson from the Carnegie Institute for Science were greatly valued. This work was supported by Academy of Finland grants 252652 and 305663.

References

Albarede, F., 1992. How deep do common basaltic magmas form and differentiate? J. Geophys. Res. Solid Earth 97 (B7), 10997–11009.
Arndt, N.T., Christensen, U., 1992. The role of lithospheric mantle in continental flood volcanism: thermal and geochemical constraints. J. Geophys. Res. Solid Earth 97 (B7), 10967–10981.
Bicca, M.M., Philipp, R.P., Jelinek, A.R., Ketzer, J.M.M., dos Santos Scherer, C.M., Jamal, D.L., dos Reis, A.D., 2017. Permian-Early Triassic tectonics and stratigraphy of the Karoo Supergroup in northwestern Mozambique. J. Afr. Earth Sci. 130, 8–27.
Bohrson, W.A., Spera, F.J., 2001. Energy-constrained open-system magmatic processes II: Application of energy-constrained assimilation-fractional crystallization (EC-AFC) model to magmatic systems. J. Petrol. 42 (5), 1019–1041.
Boyet, M., Carlson, R.W., 2006. A new geochemical model for the Earth's mantle inferred from ^{146}Sm–^{142}Nd Systematics. Earth Planet. Sci. Lett. 250 (1–2), 254–268.
Boyet, M., Blichert-Toft, J., Rosing, M., Storey, M., Télouk, P., Albaréde, F., 2003. ^{142}Nd evidence for early Earth differentiation. Earth Planet. Sci. Lett. 214 (3–4), 427–442.
Bristow, J.W., 1984. Picritic rocks of the north Lebombo and south-east Zimbabwe. Geol. Soc. South Afr. Spl. Pub. 13, 295–330.
Burke, K., Dewey, J.F., 1973. Plume-generated triple junctions: Key indicators in applying plate tectonics to old rocks. J. Geol. 81 (4), 406–433.
Campbell, I.H., Griffiths, R.W., 1990. Implications of mantle plume structure for the evolution of flood basalts. Earth Planet. Sci. Lett. 99 (1-2), 79–93. https://doi.org/10.1016/0012-821X(90)90072-6.

Caro, G., Bourdon, B., 2010. Non-chondritic Sm/Nd ratio in the terrestrial planets: Consequences for the geochemical evolution of the mantle-crust system. Geochim. Cosmochim. Acta 74 (11), 3333–3349.

Catuneanu, O., Wopfner, H., Eriksson, P.G., Cairncross, B., Rubidge, B.S., Smith, R.M.H., Hancox, P.J., 2005. The Karoo basins of south-central Africa. J. Afr. Earth Sci. 43, 211–253.

Coltice, N., Bertrand, H., Rey, P., Jourdan, F., Phillips, B.R., Ricard, Y., 2007. Global warming of the mantle beneath continents back to the Archaean. Gondwana Res. 15 (3–4), 254–266.

Cox, K.G., 1988. The Karoo province. Published in Continental flood basalts, MacDougall, J.D. Kluwer Academic Publishers, Drodrecht, pp. 239–271.

DePaolo, D.J., 1981. Trace element and isotopic effects of combined wallrock assimilation and fractional crystallization. Earth Planet. Sci. Lett. 53 (2), 189–202.

Duncan, A.R., 1987. The Karoo igneous province – a problem area for inferring tectonic setting from basalt geochemistry. J. Volcanol. Geotherm. Res. 32 (1–3), 13–34.

Duncan, A.R., Armstrong, R.A., Erlank, A.J., Marsh, J.S., Watkins, R.T., 1990. MORB-related dolerites associated with the final phases of Karoo flood basalt volcanism in southern Africa. In: Parker, A.J., Rickwood, P.C., Tucker, D.H. (Eds.), Published in Mafic Dykes and Emplacement Mechanisms. Balkema, Rotterdam, pp. 119–129.

Duncan, R.A., Hooper, P.R., Rehacek, J., Marsh, J.S., Duncan, A.R., 1997. The timing and duration of the Karoo igneous event, southern Gondwana. J. Geophys. Res. Solid Earth https://doi.org/10.1029/97JB00972.

Eglington, B.M., Armstrong, R.A., 2003. Geochronological and isotopic constraints on the Mesoproterozoic Namaqua-Natal Belt: evidence from deep borehole intersections in South Africa. Precambrian Res. 125, 179–189.

Ellam, R.M., 2006. New constraints on the petrogenesis of the Nuanetsi picrite basalts from Pb and Hf isotope data. Earth Planet. Sci. Lett. 245 (1–2), 153–161.

Ellam, R.M., Cox, K.G., 1989. A Proterozoic lithospheric source for Karoo magmatism: evidence from the Nuanetsi picrites. Earth Planet. Sci. Lett. 92, 207–218.

Ellam, R.M., Cox, K.G., 1991. An interpretation of Karoo picrite basalts in terms of interaction between asthenospheric magmas and the mantle lithosphere. Earth Planet. Sci. Lett. 105, 330–342.

Ellam, R.M., Carlson, R.W., Shirey, S.B., 1992. Evidence from Re-Os isotopes for plume-lithosphere mixing in Karoo flood basalt genesis. Nature 359, 718–721.

Fernandes, P., Cogne, N., Chew, D.M., Rodrigues, B., Jorge, R.C.G.S., Marques, J., Jamal, D., Vasconcelos, L., 2015. The thermal history of the Karoo Moatize-Minjova Basin, Tete Province, Mozambique: an integrated vitrinite reflectance and apatite fission track thermochronology study. J. Afr. Earth Sci. 112, 55–72.

Fitton, J.G., 2007. The OIB paradox. In: Foulger, G.R., Jurdy, D.M. (Eds.), Plates, Plumes, and the Planetary Processes: The Geological Society of America Special Paper. 430, pp. 387–412.

Fitton, J.G., Saunders, A.D., Norry, M.J., Hardarson, B.S., Taylor, R.N., 1997. Thermal and chemical structure of the Iceland plume. Earth Planet. Sci. Lett. 153, 197–208.

Fleming, T.H., Elliot, D.H., Jones, L.M., Bowman, J.R., Siders, M.A., 1992. Chemical and isotopic variation in an iron-rich lava flow from the Kirkpatrick Basalt, north Victoria Land, Antarctica: implications for low-temperature alteration. Contrib. Mineral. Petrol. 111 (4), 440–457.

French, S.W., Romanowicz, B., 2015. Broad plumes rooted at the base of the Earth's mantle beneath major hotspots. Nature 525, 95–99.

Gibson, S.A., Thompson, R.N., Dickin, A.P., Leonardos, O.H., 1995. High-Ti and low-Ti mafic potassic magmas: Key to plume-lithosphere interactions and continental flood-basalt genesis. Earth Planet. Sci. Lett. 136 (3–4), 149–165.

Green, D.H., Falloon, T.J., 1998. Pyrolite: a Ringwood concept and its current expression. In: Jackson, I. (Ed.), Publsihed in The Earth's Mantle: Composition, Structure, and Evolution. Cambridge University Press, pp. 311–378.

Hanyu, T., Tatsumi, Y., Senda, R., Miyazaki, T., Chang, Q., Hirahara, Y., Takahashi, T., Kawabata, H., Suzuki, K., Kimura, J.-I., Nakai, S., 2011. Geochemical characteristics and origin of the HIMU reservoir: a possible mantle plume source in the lower mantle. Geochem. Geophys. Geosyst. 12 (2). https://doi.org/10.1029/2010GC003252.

Harris, C., le Roux, P., Cuchrane, R., Martin, L., Duncan, A.R., Marsh, J.S., le Roex, A.P., Class, C., 2015. The oxygen isotope composition of Karoo and Etendeka picrites: High δ18O mantle or crustal contamination? Contrib. Mineral. Petrol. 170, 8.

Hastie, W.W., Watkeys, M.K., Aubourg, C., 2014. Magma flow in dyke swarms of the Karoo LIP: Implications for the mantle plume hypothesis. Gondwana Res. 25, 736–755.

Heinonen, J.S., Kurz, M.D., 2015. Low-^{3}He/^{4}He sublithospheric mantle source for the most magnesian magmas of the Karoo large igneous province. Earth Planet. Sci. Lett. 426, 305–315.

Heinonen, J.S., Luttinen, A.V., 2008. Jurassic dikes of Vestfjella, western Dronning Maud Land, Antarctica: geochemical tracing of ferropicrite sources. Lithos 105, 347–364.

Heinonen, J.S., Luttinen, A.V., 2010. Mineral chemical evidence for extremely magnesian subalkaline melts from Antarctic extension of the Karoo large igneous province. Mineral. Petrol. 99, 201–217.

Heinonen, J.S., Carlson, R.W., Luttinen, A.V., 2010. Isotopic (Sr, Nd, Pb. and Os) composition of highly magnesian dikes of Vestfjella, western Dronning Maud Land, Antarctica: a key to the origins of the Jurassic Karoo large igneous province? Chem. Geol. 277 (3–4), 227–244.

Heinonen, J.S., Luttinen, A.V., Riley, T.R., Michallik, R.M., 2013. Mixed pyroxenite-peridotite sources for mafic and ultramafic dikes from the Antarctic segment of the Karoo continental flood basalt province. Lithos 177, 366–380.

Heinonen, J.S., Carlson, R.W., Riley, T.R., Luttinen, A.V., Horan, M.F., 2014. Subduction-modified oceanic crust mixed with a depleted mantle reservoir in the sources of the Karoo continental flood basalt province. Earth Planet. Sci. Lett. 394, 229–241.

Heinonen, J.S., Jennings, E.S., Riley, T.R., 2015. Crystallisation temperatures of the most Mg-rich magmas of the Karoo LIP on the basis of Al-in-olivine thermometry. Chem. Geol. 411, 26–35.

Heinonen, J.S., Luttinen, A.V., Bohrson, W.A., 2016. Enriched continental flood basalts from depleted mantle melts: modeling the lithospheric contamination of Karoo lavas from Antarctica. Contrib. Mineral. Petrol. 171, 9.

Heinonen, J.S., Luttinen, A.V., Whitehouse, M.J., 2018. Enrichment of ^{18}O in the mantle sources of the Antarctic portion of the Karoo large igneous province. Contrib. Mineral. Petrol. 173, 21.

Herzberg, C., Asimow, P.D., 2008. Petrology of some oceanic island basalts: PRIMELT2.xls software for primary magma calculation. Geochem. Geophys. Geosyst. 9 (9). https://doi.org/10.1029/2008GC002057.

Herzberg, C., O'Hara, M.J., 2002. Plume-associated ultramafic magmas of Phanerozoic age. J. Petrol. 43 (10), 1857–1883.

Herzberg, C., Asimow, P.D., Arndt, N., Niu, Y., Lesher, C.M., Fitton, J.G., Cheadle, M.J., Saunders, A.D., 2007. Temperatures in ambient mantle and plumes: Constraints from basalts, picrites, and komatiites. Geochem. Geophys. Geosyst. 8 (2). https://doi.org/10.1029/2006GC001390.

Howarth, G.H., Harris, C., 2017. Discriminating between pyroxenite and peridotite sources for continental flood basalts (CFB) in southern Africa using olivine chemistry. Earth Planet. Sci. Lett. 475, 143–151.

Jackson, M.G., Carlson, R.W., 2011. An ancient recipe for flood-basalt genesis. Nature 476, 316–319.

Jackson, M.G., Jellinek, A.M., 2013. Major and trace element composition of the high ^{3}He/^{4}He mantle: Implications for the composition of a nonchondritic Earth. Geochem. Geophys. Geosyst. 14 (8). https://doi.org/10.1002/ggge.20188.

Jackson, M.G., Carlson, R.W., Kurz, M.D., Kempton, P.D., Francis, D., Blusztajn, J., 2010. Evidence for the survival of the oldest terrestrial mantle reservoir. Nature 466, 853–856.

Jacobs, J., Pisarevsky, S., Thomas, R.J., Becker, T., 2008. The Kalahari Craton during assembly and dispersal of Rodinia. Precambrian Res. 160, 142–158.

Jacobsen, S.B., Wasserburg, G.J., 1980. Sm-Nd isotopic evolution of chondrites. Earth Planet. Sci. Lett. 50 (1), 139–155.

Johnson, D.M., Hooper, P.R., Conrey, R.M., 1999. XRF analysis of rocks and minerals for major and trace elements on a single low dilution Li-tetraborate fused bead. Adv. X-ray Anal. 41, 843–867.

Jourdan, F., Féraud, G., Bertrand, H., Kampunzu, A.B., Tshoso, G., Watkeys, M.K., Le Gall, B., 2005. Karoo large igneous province: Brevity, origin, and relation to mass extinction questioned by new 40Ar/39Ar age data. Geology 33, 745–748.

Jourdan, F., Féraud, G., Bertrand, H., Watkeys, M.K., Kampunzu, A.B., Le Gall, B., 2006. Basement control on dyke distribution in Large Igneous Provinces: Case study of the Karoo triple junction. Earth Planet. Sci. Lett. 241, 307–322.

Jourdan, F., Bertrand, H., Schärer, U., Blichert-Toft, J., Féraud, G., Kampunzu, A.B., 2007. Major and trace element and Sr, Nd, Hf, and Pb isotope compositions of the Karoo large igneous province, Botswana-Zimbabwe: Lithosphere vs mantle plume contribution. J. Petrol. 48 (6), 1043–1077.

Jourdan, F., Féraud, G., Bertrand, H., Watkeys, M.K., Renne, P.R., 2008. The ^{40}Ar/^{39}Ar ages of the sill comples of the Karoo large igneous province: Implications for the Pliensbachian-Toarcian climate change. Geoghem Geophys Geosyst 9 (6). https://doi.org/10.1029/2008GC001994.

Kamenetsky, V.S., Crawford, A.J., Meffre, S., 2001. Factors controlling chemistry og magmatic spinel: an empirical study of associated olivine, Cr-spinel and melt inclusions from primitive rocks. J. Petrol. 42 (4), 655–671.

Kamenetsky, V.S., Maas, R., Kamenetsky, M.B., Yaxley, G.M., Ehrig, K., Zellmer, G.F., Bindeman, I.N., Sobolev, A.V., Kuzmin, D.V., Ivanov, A.V., Woodehead, J., Schilling, J.-G., 2017. Multiple mantle sources of continental magmatism: Insights from "high-Ti picrites" of Karoo and other large igneous provinces. Chem. Geol. 455, 22–31.

Knaack, C., Cornelius, S., Hooper, P., 1994. Trace Element Analyses of Rocks and Minerals by ICP-MS. Washington State University.

Koistinen, T., Lehtonen, M.I., Fernando, S., Matola, R., 2008. Contribution to the structure at the Eastern margin of the Archaean Zimbabwe Craton, Mozambique. Geol. Surv. Finland Spec. Pap. 48, 121–144.

Le Bas, M.J., 2000. IUGS Reclassification of the high-Mg and picritic volcanic rocks. J. Petrol. 41 (10), 1467–1470.

Le Roux, V., Dasgupta, R., Lee, C.-T.A., 2011. Mineralogical heterogeneities in the Earth's mantle: Constraints from Mn, Co, Ni and Zn partitioning during partial melting. Earth Planet. Sci. Lett. 307 (3–4), 395–408.

Luttinen, A.V., 2018. Bilateral geochemical asymmetry in the Karoo large igneous province. Sci. Rep. 8. https://doi.org/10.1038/s41598-018-23661-3.

Luttinen, A.V., Furnes, H., 2000. Flood basalts of Vestfjella: Jurassic magmatism across an Archean-Proterozoic lithospheric boundary in Dronning Maud Land, Antarctica. J. Petrol. 41 (8), 1271–1305.

Luttinen, A.V., Rämö, O.T., Huhma, H., 1998. Neodymium and strontium isotopic and trace element composition of a Mesozoic CFB suite from Dronning Maud Land, Antarctica: implications for lithosphere and asthenosphere contributions to Karoo magmatism. Geochim. Cosmochim. Acta 62 (15), 2701–2714.

Luttinen, A.V., Heinonen, J.S., Kurhila, M., Jourdan, F., Mänttäri, I., Vuori, S.K., Huhma, H., 2015. Depleted mantle-sourced CFB magmatism in the Jurassic Africa-Antarctica rift: Petrology and ^{40}Ar/^{39}Ar and U/Pb chronology of the Vestfjella dyke swarm, Dronning Maud Land, Antarctica. J. Petrol. 56 (5), 919–952.

Maclennan, J., 2008. Lead isotope variability in olivine-hosted melt inclusions from Iceland. Geochim. Cosmochim. Acta 72, 4159–4176.

Manninen, T., Eerola, T., Mäkitie, H., Vuori, S., Luttinen, A., Sénvano, A., Manhiça, V., 2008. The Karoo volcanic rocks and related intrusions in Southern and Central Mozambique. Geol. Surv. Finland Spec. Pap. 48, 211–250.

Matzen, A.K., Wood, B.J., Baker, M.B., Stolper, E.M., 2017. The roles of pyroxenite and peridotite in the mantle sources of oceanic basalts. Nat. Geosci. 10, 530–535.

Maurel, C., Maurel, P., 1982. Etude experimentale de equilibre Fe^{2+}– Fe^{3+} dans les spinelles chromiferes at les liquides silicates basiques coexistants, a 1 atm. Compt. Rendus Ac. Sci. 295, 209–212.
Melluso, L., Cucciniello, C., Petrone, C.M., Lustrino, M., Morra, V., Tiepolo, M., Vasconcelos, L., 2008. Petrology of Karoo volcanic rocks in the southern Lebombo monocline, Mozambique. J. Afr. Earth Sci. 52 (4–5), 139–151.
Michael, P., 1995. Regionally distinctive sources of depleted MORB: evidence from trace elements and H_2O. Earth Planet. Sci. Lett. 131 (3–4), 301–320.
Moyes, A.B., Krynauw, J.R., Barton, J.M.J.N.R., 1995. The age of the Ritscherflya Supergroup and Borgmassivet Intrusions, Dronning Maud Land, Antarctica. Antarctic Sci. 7 1, 87–97.
Neumann, E.-R., Svensen, H., Galerne, C.Y., Planke, S., 2011. Multistage evolution of dolerites in the Karoo large igneous province, Central South Africa. J. Petrol. 52 (5), 959–984.
Oesterlen, P.M., Millsteed, B.D., 1994. Lithostratigraphy, palaentology, and sedimentary environments of the western Cabora Bassa Basin, Lower Zambezi Valley, Zimbabwe. S. Afr. J. Geol. 97 (2), 205–224.
O'Nions, R.K., Hamilton, P.J., Evensen, N.M., 1977. Variations in $^{143}Nd/^{144}Nd$ and $^{87}Sr/^{86}Sr$ ratios in oceanic basalts. Earth Planet. Sci. Lett. 34 (1), 13–22.
Pertermann, M., Hirschmann, M.M., Hametner, K., Günther, D., Schmidt, M.W., 2004. Experimental determination of trace element partitioning between garnet and silica-rich liquid during anhydrous partial melting of MORB-like eclogite. Geochem. Geophys. Geosyst. https://doi.org/10.1029/2003GC000638.
Putirka, K.D., Perfit, M., Ryerson, F.J., Jackson, M.G., 2007. Ambient and excess mantle temperatures, olivine thermometry, and active vs. passive upwelling. Chem. Geol. 241 (3–4), 177–206.
Puttonen, R., 2016. Keski-Mosambikin jurakautisten ryoliittien U-Pb zirkoniänmääritykset ja Lu-Hf-isotooppikoostumus: viitteitä monivaiheisesta felsisestä Karoo-magmatismista. (Unpublished Master's thesis). Department of Geosciences and Geography, University of Helsinki.
Riley, T.R., Leat, P.T., Curtis, M.L., Millar, I.L., Duncan, R.A., Fazel, A., 2005. Early–middle Jurassic dolerite dykes from Western Dronning Maud land (Antarctica): Identifying mantle sources in the Karoo large igneous province. J. Petrol. 46, 1489–1524.
Simkin, T., Smith, J.V., 1970. Minor-element distribution in olivine. J. Geol. 78, 304–325.
Smith, R.M.H., 1990. A review of stratigraphy and sedimentary environments of the Karoo Basin of South Africa. J. Afr. Earth Sci. (and the Middle East) 10 (1–2), 117–137.
Sobolev, A.V., Shimizu, N., 1993. Ultra-depleted primary melt included in an olivine from the Mid-Atlantic Ridge. Nature 363, 151–154.
Sobolev, A.V., Hofmann, A.W., Kuzmin, D.V., Yaxley, G.M., Arndt, N.T., Chung, S.-L., Danyushevsky, L.-V., Elliott, T., Frey, F.A., Garcia, M.O., Gurenko, A.A., Kamenetsky, V.A., Kerr, A.C., Krivolutskaya, N.A., Matvienkov, V.V., Nikogosian, I.K., Rocholl, A., Sigurdsson, I.A., Suschevskaya, N.M., Teklay, M., 2007. The amount of recycled crust in sources of mantle-deried melts. Science 316 (5823), 412–417.
Storey, B.C., 1995. The role of mantle plumes in continental breakuop: case histories from Gondwanaland. Nature 377, 301–308.
Sun, S.S., McDonough, W.F., 1989. Chemical and isotopic systematic of oceanic basalts: implications for mantle compositions and processes. Geol. Soc. London, Spl. Pub. 42, 313–345.
Svensen, H., Corfu, F., Polteau, S., Hammer, Ø., Planke, S., 2012. Rapid magma emplacement in the Karoo large igneous province. Earth Planet. Sci. Lett. 325–326, 1–9.
Sweeney, R.J., Duncan, A.R., Erlank, A.J., 1994. Geochemistry and petrogenesis of Central Lebombo basalts of the Karoo igneous province. J. Petrol. 35 (1), 95–125. https://doi.org/10.1093/petrology/35.1.95.
Sweeney, R.J., Falloon, T.J., Green, D.H., Tatsumi, Y., 1991. The mantle origins of Karoo picrites. Earth Planet. Sci. Lett. 107 (2), 256–271.
Tanaka, T., Togashi, S., Kamioka, H., Amakawa, H., Kagami, H., Hamamoto, T., Yuhara, M., Orihashi, Y., Yoneda, S., Shimizu, H., Kunimaru, T., Takahashi, K., Yanagi, T., Nakano, T., Fujimaki, H., Shinjo, R., Asahara, Y., Tanimizu, M., Dragusanu, C., 2000. JNdi-1: a neodymium isotopic reference in concistency with LaJolla neodymium. Chem. Geol. 168 (3–4), 279–281.
Thompson, R.N., Gibson, S.A., 2000. Transient high temperatures in mantle plume heads inferred from magnesian olivines in Phanerozoic picrites. Nature 407, 502–506.
Tolstikhin, I., Hofmann, A.W., 2005. Early crust on top of the Earth's core. Phys. Earth Planet. Inter. 148, 109–130.
Torsvik, T.H., Burke, K., Steinberger, B., Webb, S.J., Ashwal, L.D., 2010. Diamonds sampled by plumes from the core-mantle boundary. Nature 466, 352–355.
Walter, M.J., 1998. Melting of garnet peridotite and the origin of komatiite and depleted lithosphere. J. Petrol. 39, 29–60.
Wang, X.-C., Wilde, S.A., Li, Q.-L., Yang, Y.-N., 2015. Continental flood basalts derived from the hydrous mantle transition zone. Nature Commun. 6, 7700.
Wedepohl, K.H., 1995. The composition of continental crust. Geochim. Cosmochim. Acta 59 (7), 1217–1232.
White, R.S., 1997. Mantle plume origin for the Karoo and Ventersdorp flood basalts, South Africa. S. Afr. J. Geol. 100 (4), 271–282.
Willbold, M., Stracke, A., 2010. Formation of enriched mantle components by recycling of upper and lower continental crust. Chem. Geol. 276 (3-4), 188–197. https://doi.org/10.1016/j.chemgeo.2010.06.005.
Workman, R.K., Hart, S.R., 2005. Major and trace element composition of the depleted MORB mantle (DMM). Earth Planet. Sci. Lett. 231 (1-2), 53–72.
Zindler, A., Hart, S., 1986. Chemical geodynamics. Annu. Rev. Earth Planet. Sci. 14, 493–571.